TITLE

The BRCA1- RAD51 Axis Regulates SCAI/REV3 Dependent Replication Fork Maintenance

AUTHOR LIST

Chloe Unterseher[1, #], Hiroshi Tsuchida[1, #], Rosevalentine Bosire[1], Xuhui Jin[1], Shaylee Kieffer[1] and Richard O. Adeyemi[1,2*]

AFFILIATIONS

[1]Basic Sciences Division, Fred Hutchinson Cancer Center, Seattle, WA 98109
[2]Department of Biochemistry, University of Washington, Seattle WA 98195

# These authors contributed equally.

* Corresponding author:
Richard Adeyemi, D.V.M., Ph.D.,
Basic Sciences Division, Fred Hutchinson Cancer Center,
1100 Fairview Ave, Mail Stop A1-162, Seattle, WA 98109, U.S.A.
Phone (office): (206)667-6263
Email: radeyemi@fredhutch.org

ABSTRACT

Replication stress is a key contributor to genomic instability and cancers. BRCA1 has well established roles in protecting stalled forks against degradation. Here we show that BRCA1 has a fork protection-independent role in driving stalled forks restoration via regulation of RAD51 in a manner that confers dependency on SCAI and REV3. BRCA1 drives SLX4-mediated DNA break formation in the absence of SCAI and REV3, which are required to complete repair synthesis and fork restart. Domain analysis revealed that the increased fork breakage seen in the absence of SCAI requires the coiled coil domain of BRCA1 and is regulated in a manner distinct from BRCA1's roles in resection control at two-ended double strand breaks. BRCA1's role also occurs independently of 53BP1 but is modulated by RIF1. Surprisingly, loss of fork reversal factors leads to increased fork breakage in the absence of SCAI/REV3 in a manner that depends on RAD51 activity. SCAI loss leads to persistent DNA breaks, genomic instability and cell death upon DNA damage. We posit that SCAI/REV3 may be required to replicate through and rescue stalled replication forks at fragile genomic regions. Failure to do so leads to increased DNA breakage and genomic instability.

Keywords: DNA repair, replication stress, homologous recombination, BRCA1, RAD51, REV3, SCAI, 53BP1, RIF1, SMARCAL1, SLX4, fork reversal, fork restart, fork collapse

INTRODUCTION

Faithful duplication of the genome of dividing cells is continually threatened by impediments that challenge replication fork progression [1]. Such obstacles can result from lesions arising from exogenous DNA damage or from endogenous sources such as DNA secondary structures, difficult-to-replicate chromatin, oncogene-driven hyper-replication, and transcription-replication conflicts, among others [2]. Collectively, these inputs result in replication stress and, if left unresolved, drive fork stalling, breakage, and collapse with subsequent genome instability—a key hallmark of several cancers [3, 4]. To avert these outcomes, cells deploy a coordinated replication-stress response that stabilizes perturbed forks, remodels fork architecture, and re-establishes DNA synthesis through pathway choices that include repriming, translesion synthesis (TLS), template switching, and recombination-based restart [5].

A central remodeling route at stalled forks is fork reversal—conversion of the stalled fork into a four-way duplex intermediate—catalyzed by annealing helicases/ATP-dependent translocases such as SMARCAL1, ZRANB3, and others [6, 7]. Fork reversal can protect against further damage, yet reversed forks are intrinsically vulnerable. Homologous recombination (HR) factors, most notably RAD51 and BRCA1/BRCA2, extend their canonical roles beyond two-ended double strand break (DSB) repair to stabilize and protect nascent strands at reversed forks and to promote efficient restart [8, 9]. However, the varied functions of these proteins at stalled forks and how these differ from conventional two-ended breaks is still not clear.

In addition, how stalled forks transition back to productive replication remains an area of active investigation [10, 11]. In addition to RAD51's fork protective function, several studies have shown that RAD51 drives reversal of stalled forks and is important for promoting fork restart [12, 13]. Forks can restart via repriming [14] (which suppresses fork reversal and leaves post-replicative single-stranded DNA gaps to be filled later by template switching or TLS) or via direct RECQ1 activity on reversed forks [15]. Alternatively, stalled or reversed forks can be cleaved by structure-specific endonucleases (e.g., MUS81–EME1, SLX1–SLX4), generating one-ended DSBs that are repaired via recombination-based restart [16, 17]. In mammalian cells, such restart often resembles break-induced replication (BIR)—a conservative, long-tract synthesis program that, in several contexts, operates with minimal contribution from RAD51's strand-exchange activity [18, 19]. Alternatively, RAD51 dependent recombination restart mechanisms without break formation have also been proposed [20, 21].

We previously identified a general requirement for the Protexin complex—comprising SCAI and the Pol ζ catalytic subunit REV3—in promoting viability after replicative damage [22]. In particular, we uncovered a TLS-independent function of SCAI/REV3 in the response to DNA interstrand crosslinks (ICLs), where SCAI restrains excessive EXO1-mediated resection and preserves replication competence. These findings, however, suggested that SCAI/REV3 does more than modulate a single nuclease axis at ICLs; rather, it raised the possibility that SCAI/REV3 integrates multiple dimensions of stalled-fork metabolism. Here, we investigate how the SCAI/REV3 complex regulates

fork progression after replication stress and how the complex interfaces with the RAD51/BRCA1 module to govern outcomes at stalled forks. We show that SCAI/REV3 is required to sustain DNA synthesis during replication stress and to promote efficient fork restart. Strikingly, in the absence of SCAI, there is increased replication stress associated fork breakage, genomic instability and cell death. Fork breakage in the absence of SCAI/REV3 is orchestrated by BRCA1-RAD51 via SLX4 recruitment. Remarkably, SCAI loss appears to confer a dependency on fork reversal, as combined loss of SMARCAL1 and SCAI leads to increased fork breakage. We also define requirements for BRCA1's role in promoting increased breakage and resection at stalled forks and show that this occurs independent of 53BP1 regulation but is modulated by RIF1. We propose that SCAI loss causes a failure of strand invasion mediated fork restart with resultant fork breakage and genomic instability. By defining the contexts in which BRCA1 and RAD51 are required to generate restart-competent intermediates, we provide a mechanistic framework that clarifies how cells regulate repair outcomes upon fork stalling.

RESULTS

SCAI promotes integrity and efficient restart of stalled replication forks

SCAI demonstrably regulates stalled replication fork resection [22, 23]; however, we also previously found that EXO1 loss only partially rescues viability in the absence of SCAI, suggesting that SCAI might perform other roles at stalled forks beyond EXO1 regulation. One such role could be in the regulation of stalled fork processing and restart. Using BrdU incorporation assays, we have previously observed reduced incorporation of BrdU correlating to reduced DNA synthesis rates following release from hydroxyurea (HU)-induced fork stalling when SCAI was depleted [22], suggesting that SCAI might be important regulating fork recovery and progression after prolonged stalling. To directly investigate SCAI's role in replication fork dynamics, we assayed for potential fork restart defects in the absence of SCAI using the single molecule DNA fiber technique. Although there is no clear consensus on which factors are key for promoting restart, previous work has shown that fork restart following HU treatment is differentially regulated depending on the duration of fork stalling [13, 24]. Thus, we first tested whether SCAI might modulate restart under acute (2 hour) treatment conditions with a moderate dose of HU in RPE1 cells. Under these conditions, we failed to detect any differences in either fork restart efficiency, number of stalled forks, or new origin firing (Figure S1A). Similar results were observed following depletion of SCAI's binding partner, REV3 (Figure S1A).

A typical S-phase lasts for close to 8 hours with some regions of the genome replicated late in the cycle. Prolonged fork stalling (8 plus hours) often leads to fork breakage and RAD51 dependent restart mechanisms [20, 25]. We reasoned that SCAI might be important for modulating repair outcomes upon prolonged replication stress. To test this, we examined fork dynamics upon treatment with HU for 18 h. In this experimental setup, because we were making use of an HU dose that does not completely block DNA synthesis, and to allow for adequate tracking of restarted forks, the green label was kept during the period of HU treatment. We observed that SCAI loss led to reduced lengths of the second, red-labeled fibers suggesting that there was defective fork restart in the absence of SCAI (Figure 1A, right panel). Knockdown of

131 REV3 also led to reduction in fork restart efficiency (Figure 1A, right panel). Because
132 SCAI loss did not affect green fiber lengths under short HU treatment conditions (Figure
133 S1A), our observation that SCAI/REV3 loss also caused reduced lengths of the green
134 label under prolonged replication stress (Figure 1A, left panel) suggested that fork
135 progression during or following conditions of replication stress was also compromised
136 by loss of SCAI. To further understand SCAI's role in regulating fork progression under
137 replication stress conditions, we switched our labeling strategy to introduce the second
138 label along with HU treatment. Under these HU treatment conditions, the replicative
139 forks advanced over 30 times slower compared to untreated conditions, such that 18-
140 hour treatment led to about half the fork advancement as the initial 30-minute pulse
141 (Figure 1B). Nevertheless, SCAI loss consistently led to reduced fork progression upon
142 replicative stress induction (Figure 1B, right panels). SCAI loss affected fiber length
143 whenever cells were undergoing replication stress both in dual-labeled (restarted)
144 (Figure 1B, top panels) or single labeled (Figure 1B, lower panels) conditions.
145 It is known that fork stalling can lead to fork reversal with subsequent fork
146 degradation [7, 26, 27]. Furthermore, we and others have previously reported that SCAI
147 regulates EXO1 activity and degradation of stalled forks [22, 23]. These experiments
148 are typically performed following absolute blocks to fork advancement. Notably, SCAI
149 loss did not affect the length of green only fibers prior to HU treatment under these
150 conditions (Figure 1B), suggesting this effect was not due to fork degradation.
151 Nevertheless, to determine whether the reduced fork progression in the absence of
152 SCAI was a result of increased fork degradation, we co-depleted EXO1 and SCAI and
153 performed similar DNA fiber assays. As expected, SCAI loss led to reduction fork
154 progression upon replication stress (Figure 1C, right panel) without affecting
155 progression under untreated conditions (Figure 1C, left panel). Importantly, rather than
156 rescue reduced fork lengths, co-depletion of EXO1 had no effect on fork progression in
157 the absence of SCAI (Figure 1C, left and right panels). Taken together, these results
158 demonstrate that SCAI was required for adequate fork progression upon replication
159 stress and for proper restart of stalled forks. This function of SCAI is independent of its
160 role in EXO1 regulation.
161
162 **SCAI/REV3 limit fork breakage following replication fork stalling**
163 Compromised fork progression under replicative stress may result from
164 increased fork breakage and/or collapse, increased fork reversal, or a combination of
165 these [28-30]. Altered replicative stress signaling can imply fork breakage. To examine
166 how loss of SCAI impacted replication fork stalling, RPE1 cells were transfected with
167 two different siRNAs to SCAI. Subsequently, forks were stalled using similar HU
168 conditions as in previous experiments and blotted for replication stress markers. As
169 expected, and consistent with what was observed following treatment with crosslinking
170 agents [22], SCAI loss led to increases in CHK1 and RPA phosphorylation (Figure 2A).
171 Importantly, upon SCAI depletion with either siRNA, we observed significantly increased
172 phosphorylation of H2AX (hereafter γH2AX), typically a marker of double-stranded DNA
173 breaks, without any changes to H2AX protein amounts (Figure 2A). To further examine
174 this, we made use of U2OS cells engineered to knock out SCAI using CRISPR. In this
175 cell type, we observed similar increases in γH2AX and RPA phosphorylated on S4/8
176 (hereafter pRPA) levels, another marker of replication-associated fork breakage [31, 32]

177 (Figure 2B). Upon HU treatment, the increased pRPA in ΔSCAI cells could be rescued
178 by re-introducing SCAI (Figure 2C, compare lanes 2, 4 & 6), confirming that the
179 increased fork breakage was due to SCAI loss. Next, we performed a time course
180 analysis to determine at which point fork breakage occurs in the absence of SCAI. We
181 had earlier failed to observe any effect of SCAI loss on fork restart after treatment with
182 HU for 2 h (Figure S1A). Although SCAI loss led to slightly increased pChk1 at 4 h after
183 HU treatment (Figure S2A, lanes 3 & 4), γH2AX and pRPA levels remained unchanged
184 relative to controls (Figure S2A). However, by 18 hours, there was marked increase in
185 γH2AX and pRPA levels, suggesting SCAI loss results in increased fork breakage upon
186 prolonged fork stalling (Figure S2A).
187 To further explore SCAI's function during replication stress and to make sure this
188 effect was not unique to HU treatment, we examined SCAI's role upon treatment with
189 aphidicolin, a DNA polymerase alpha inhibitor that also causes replication stress and
190 fork stalling [33, 34]. Similar to what was observed following HU treatment, SCAI
191 depletion led to increased γH2AX and pRPA upon treatment with aphidicolin (Figure
192 2D), showing that this altered signaling resulted from SCAI dependency at distressed
193 forks. To directly examine altered fork breakage upon SCAI loss, we performed neutral
194 comet assays. Consistent with the Western blotting data, depletion of SCAI led to
195 significant increases in fork breakage upon replication stress compared to controls in
196 both RPE1 (Figure 2E) and U2OS cells (Figure 2F). Taken together, these data shows
197 that SCAI loss results in compromised fork progression and increased fork breakage
198 under replication stress.
199 To examine whether REV3 shared similar roles with SCAI in preventing fork
200 breakage at HU stalled forks, we depleted REV3 using siRNAs. Similar to what was
201 observed upon SCAI loss, REV3 depletion led to increases in pRPA and γH2AX upon
202 fork stalling (Figure 2G, compare lanes 2 and 4), suggesting a similar function for REV3
203 in preventing fork breakage. Because HU does not directly lead to formation of DNA
204 adducts, this role appeared to be independent of REV3's role in TLS across damaged
205 DNA bases. To further examine this, we depleted cells of REV7, which is critical for TLS
206 as a component of DNA polymerase zeta [35]. Whereas REV3 loss led to increases in
207 pRPA and γH2AX after HU treatment, REV7 depletion (and thus inhibition of TLS) did
208 not (Figure 2G, compare lanes 4 and 6). To directly test whether failure of TLS would
209 result in increased fork breakage we treated cells with a previously reported TLS
210 inhibitor [36]. Similar to REV7 depletion, TLS inhibition failed to increase pRPA and
211 γH2AX after replication stress (Figure S2B) suggesting that increased fork breakage in
212 the absence of REV3 was not attributable to a TLS function of REV3. Depletion of
213 REV3 in SCAI knockout (KO) cells did not significantly alter the amounts of pRPA and
214 γH2AX, suggesting that both proteins function in the same pathway (Figure S2C). As a
215 direct marker of fork breakage, neutral comet assays showed that REV3 loss led to
216 increased fork breakage, as did loss of SCAI (Figure 3G).
217 As an orthogonal approach, we examined replication stress signaling events
218 using immunofluorescence (IF) microscopy. To determine whether the observed
219 increased pRPA signified increases on chromatin, cells were pre-extracted with
220 cytoskeleton buffer to remove unbound proteins. Depletion of either SCAI or REV3 led
221 to increased intensity of RPA upon HU treatment, suggesting that increased pRPA
222 occurred on chromatin (Figure S2D). We also observed increased γH2AX using this

223 approach (Figure S2E). Finally, cells knocked down for REV3 or SCAI were examined
224 for increases in chromatin-bound RPA or γH2AX using quantitative image-based
225 cytometry (QIBC). Upon HU treatment, QIBC showed increased γH2AX and RPA levels
226 indicative of increase fork breakage (Figure 2H-J).
227 Unlike ICL treatment, which typically blocks helicase unwinding, HU treatment
228 uncouples the helicase from the polymerase, thereby increasing RPA loading on the
229 resulting singe-stranded DNA (ssDNA) [37]. Thus, resection is unlikely to be the primary
230 driver of fork breakage. Since SCAI was previously shown to regulate EXO1, we
231 depleted EXO1 upon SCAI loss. Notably, and contrary to what was seen following
232 treatment with ICL agents [22], the increases in pRPA seen after HU treatment could not
233 be reversed by knockdown of EXO1 (Figure S2F) further demonstrating that SCAI
234 performs multiple roles at stalled forks and regulates stalled fork dynamics independent
235 of EXO1 regulation (see also Figure 1C).
236
237 **BRCA1 promotes increased fork breakage and resection in the absence of**
238 **SCAI/REV3**
239 We next hypothesized that BRCA1 might have a role in the increased pRPA and
240 γH2AX observed in the SCAI knockdown cells, as BRCA1 is important for resection
241 control at two ended DSBs and plays multiple roles in regulating stalled fork dynamics
242 [38, 39]. To examine the effect of BRCA1, we made use of RPE1 cell lines in which
243 BRCA1 had been eliminated using CRISPR and examined for alteration in pRPA and
244 γH2AX levels. As expected, SCAI depletion led to increased fork breakage upon HU
245 treatment (Figure 3A, compare lanes 2 & 3) in BRCA1 proficient RPE1 cells. Strikingly,
246 we observed that loss of BRCA1 abolished the increased γH2AX and pRPA levels seen
247 upon SCAI loss (Figure 3A, compare lanes 3 & 5). To further examine BRCA1's role, we
248 depleted BRCA1 in RPE1 cells using siRNA. Consistent with our KO cell data, the
249 increased pRPA and γH2AX seen upon SCAI loss was eliminated upon BRCA1
250 depletion (Figure S3A). BARD1 is a key interaction partner that forms a stable complex
251 with BRCA1 [40]. To further examine a potential role for BRCA1 in regulating stalled fork
252 breakage in the absence of SCAI, we depleted cells of BARD1. As expected, BARD1
253 knockdown led to diminished levels of BRCA1 (Figure S3A). Similar to what was seen
254 upon BRCA1 loss, BARD1 knockdown eliminated the increases in pRPA and γH2AX
255 seen whenever SCAI is lost (Figure S3A). Basal levels of pRPA and γH2AX were higher
256 in BARD1 knockdown vs BRCA1 knockdown cells for unclear reasons. To see if a
257 similar effect applied to REV3, we depleted SCAI and REV3 using siRNAs in WT or
258 BRCA1 KO cells. As shown earlier, we observed increases in damage signaling
259 markers indicative of fork breakage and resection upon loss of either SCAI or REV3
260 (Figure 3B, compare lane 3 with lanes 5 & 7). Importantly, cell lines lacking BRCA1
261 failed to show such increases (Figure 3B, compare 5 & 6 and lanes 7 & 8), suggesting
262 that BRCA1 mediates fork breakage in the absence of the SCAI/REV3 complex. These
263 findings were further confirmed using IF experiments, where loss of BRCA1 led to
264 reduced amounts of RPA on chromatin as well as decreased γH2AX levels, again
265 demonstrating a key role for BRCA1 in mediating fork breakage upon SCAI/REV3 loss
266 (Figure 3C – F).
267 To directly examine if BRCA1 regulates fork breakage after SCAI/REV3
268 depletion, we performed neutral comet assays. As expected, loss of either SCAI or

269 REV3 led to increased accumulation of DNA breaks (Figure 3G). Importantly, co-
270 depletion of BRCA1 with SCAI led to failure to accumulate DNA breaks (Figure 3G),
271 suggesting that the DNA breakage seen in the absence of SCAI/REV3 was orchestrated
272 by BRCA1 activity. These results could imply that SCAI/REV3 act downstream of
273 BRCA1 activity. SCAI binds to ssDNA [41], and if BRCA1's role in this context was to
274 promote DNA resection that may allow SCAI to be recruited to damaged chromatin. To
275 examine this, we treated WT or BRCA1 deficient cells with HU and performed chromatin
276 fractionation experiments. As expected, loss of SCAI led to increased DNA break
277 formation (Figure 3H, compare lanes 2 & 3), which failed to occur in the absence of
278 BRCA1 (Figure 3H, compare lanes 3 & 5). Importantly, SCAI accumulated in chromatin
279 fractions upon HU treatment (Figure 3H, compare lanes 1 and 2) but this increase in
280 SCAI accumulation was not affected by BRCA1 loss (Figure 3H, compare lanes 2 & 4).
281 Thus, BRCA1 likely performs a different function that confers a dependency on SCAI
282 activity or compensates for loss of SCAI by inducing fork breakage.
283 Resection at ICLs and upon HU treatment is often differentially regulated [42].
284 Although SCAI's role at ICLs was more impacted by regulation of EXO1 compared to
285 HU, we wanted to determine whether the increased resection observed in the absence
286 of SCAI was regulated by BRCA1 in both contexts. Similar to what was observed with
287 HU, the cisplatin induced increase in pRPA was abolished upon BRCA1 depletion
288 (Figure S3B, compare lanes 4 & 6). This effect was also seen following depletion of
289 BARD1 (Figure S3B). It is worth noting that following either HU or cisplatin treatment,
290 BRCA1 loss did not cause similar reductions in CHK1 activation (nor does it eliminate
291 the increased CHK1 phosphorylation (pCHK1) seen upon SCAI/REV3 loss), suggesting
292 that ATR activity *per se* (which regulates damage signaling upon replication stress) was
293 not affected by loss of BRCA1 (Figure 3B and Figure S3B). Taken together, our results
294 demonstrate that BRCA1 orchestrates fork breakage in the absence of SCAI/REV3
295 upon treatment with various agents that stall and/or damage replication forks.
296
297 **BRCA1 requirements for regulating stalled fork breakage**
298 BRCA1 forms several complexes that play important roles in resection control,
299 HR and other functions; these different complexes mediate the various functions of
300 BRCA1 [43, 44]. For example, the BRCA1-CtIP complex, formed via CtIP binding to the
301 C-terminus of BRCA1, controls resection at ionizing radiation-induced DSBs [45, 46].
302 Since BRCA1 controls fork breakage and pRPA upon SCAI loss, we wanted to
303 determine which subcomplexes and function of BRCA1 was important for this role.
304 These experiments were performed either following cisplatin or HU treatment and
305 depletion of ABRA1, BRIP1 or CtIP (key members of the BRCA1-A, B or C complexes)
306 respectively. Our data showed that loss of any of these factors did not prevent
307 increased pRPA in the absence of SCAI upon cisplatin treatment (Figure S4A).
308 Repeating a similar experiment following HU treatment showed similar results:
309 increased pRPA upon SCAI loss in each condition (Figure S4B). However, we did
310 observe that depletion of Abraxas by itself increased the basal level of pRPA under HU
311 treatment conditions (Figure S4B, lane 4). Such a role for ABRA1 (Abraxas) has been
312 reported following treatment with the topoisomerase inhibitor, camptothecin [47]. Taken
313 together, our data suggests that the three major BRCA1 complexes do not account for

314 the observed SCAI-depletion phenotype, but that its obligate binding partner BARD1 is
315 involved.
316 Next, we examined domain requirements of BRCA1 for fork breakage using
317 previously reported BRCA1 mutant expressing cell lines [48]. Increased BRCA1
318 dependent fork resection upon loss of either SCAI or REV3 could be almost fully
319 rescued by reintroducing tagged WT-BRCA1 into knockout cell lines (Figure S4C). We
320 then examined the role of two domain mutants of BRCA1. First, a point mutation
321 (S1655A) in the BRCT domain of BRCA1 that abrogates its interaction with
322 phosphorylation dependent binding partners (ABRA1, BRIP1 or CtIP). A second mutant
323 deleted the C-terminal coiled coil domain that is essential for HR. As expected, BRCA1
324 deletion reduced pRPA levels (Figure 4A, lane 2). Reintroduction of the $BRCA1^{S1665A}$
325 mutant allowed restoration of fork resection to almost the same extent as seen following
326 reintroduction of WT-BRCA1 (Figure 4A, compare lanes 1 and 3), suggesting that this
327 domain was not required for the BRCA1 induced fork resection phenotype. This finding
328 is consistent with what was observed following siRNA depletion of ABRA1, BRIP1 or
329 CtIP, whose depletion failed to abrogate BRCA1's role in promoting fork resection in the
330 absence of SCAI (Figures S4A & S4B). In contrast, the coiled coil domain mutant (ΔCC)
331 of BRCA1 did not fully restore fork resection (Figure 4B, compare lanes 1 & 3)
332 suggesting that this domain was important for BRCA1's role in promoting stalled fork
333 resection. To address this fully, we performed a dose curve of HU treatment and
334 compared the ability of the WT BRCA1 and $BRCA1^{\Delta CC}$ mutants to rescue SCAI
335 dependent fork breakage and resection (Figure 4C). These data confirmed that the
336 coiled coil domain of BRCA1 was required to promote stalled fork resection and
337 breakage in the absence of SCAI (Figure 4C, compare lanes 4&5, 6&7, 8&9). Note that
338 these findings are different from the domain requirements of BRCA1 in promoting
339 resection at two-ended DSBs, where binding to CtIP through the BRCT domain is
340 critical for resection [49].
341
342 **BRCA1 pro-breakage / resection roles at stalled and broken forks occur**
343 **independently of 53BP1**
344 Previous studies have shown that BRCA1's role in resection control at two-ended
345 DSB sites is typically antagonized by 53BP1, which enforces a block to resection in the
346 absence of BRCA1 [50, 51]. BRCA1 overcomes the 53BP1 block to resection upon S
347 phase entry through newly-replicated chromatin-dependent extrusion of 53BP1 as well
348 as CDK dependent activation of CtIP [52-54]. This has implications for efficacy of
349 treatment with PARP inhibitors (PARPi), as PARPi induced cell death in the absence of
350 BRCA1 can be overcome by loss of 53BP1 [55]. Interestingly, SCAI also binds to
351 53BP1; however, the reason for this association is not fully clear although it may involve
352 regulation of RIF1 activity [56]. Fork breakage at stalled forks typically leads to single
353 but not two-ended DSBs (unless there is replisome bypass of a lagging strand nick)
354 [57], and so, to determine whether this role of BRCA1 was mediated by counteracting
355 53BP1 activity, we examined the effects of 53BP1 loss on resection control at stalled
356 forks in the absence of SCAI.
357 Since BRCA1 drives fork breakage and resection both upon fork stalling and
358 following ICL formation, we examined the phenotypes in both contexts. For simplicity,
359 we focused on changes to resection as indicated by increases in pRPA. HU leads to

uncoupling of the replicative helicase from the polymerase and thus causes higher background pRPA in the absence of any specific gene alterations (Figure S4D, lane 2). Thus, we have largely focused on describing results seen upon cisplatin treatment and how this agrees with or varies from what is observed following HU treatment. As expected, SCAI KO cells showed increases in pRPA upon cisplatin treatment (Figure 4D, compare lanes 1 and 2) that was abolished by BRCA1 depletion (Figure 4D, lane 3). HU treatment behaved similarly (Figure S4D, lanes 2, 3 & 5). Depletion of 53BP1 alone using siRNAs failed to alter pRPA levels upon cisplatin treatment (Figure 4D, lane 4). Nevertheless, co-depletion of 53BP1 and SCAI led to slight but consistent additional increases in pRPA upon cisplatin (Figure 4D, compare lanes 2 and 5) or HU (Figure S4D, compare lanes 3 and 4) treatment suggesting a role for SCAI in restraining 53BP1 in this context. If BRCA1 was relieving a 53BP1-mediated block to resection like it does at two-ended breaks, it then follows that co-depletion of 53BP1 and BRCA1 should restore the pRPA in the absence of SCAI. However, this was not the case, as BRCA1 loss not only abolished the increased resection and/or fork breakage seen in the absence of either SCAI or 53BP1, but it did so even when SCAI was co-depleted alongside 53BP1. This was seen both following cisplatin treatment (Figure 4D, lane 5 and 7) and HU treatment (Figure S4D, lanes 4 and 6, see γH2AX levels as well). Taken together, these results show thatBRCA1 mediated fork breakage and resection in the absence of SCAI is not regulated or counteracted by 53BP1 activity, dissimilar to the antagonism that occurs at two-ended DSBs.

RIF1 differentially modulates BRCA1 activity and resection at stalled forks and ICLs

At two-ended DSBs, 53BP1 orchestrates its block to end resection through downstream effectors such as RIF1, REV7 and the Shieldin complex – all of which are recruited to these breaks in a 53BP1 dependent manner [58, 59]. However, at stalled forks, RIF1 has been shown to be recruited independently of 53BP1 where it regulates stalled fork stability [60]. In fact, 53BP1 has also been linked to regulation of fork stability [61]. However, because we have data showing that BRCA1 acts differently, and without 53BP1 regulation, at stalled forks than it does at DSBs, we also wanted to determine whether RIF1 might behave differently than 53BP1 at stalled forks. To test this, first we depleted 53BP1 and RIF1 using siRNAs and examined changes to resection upon HU treatment. We observed that, while 53BP1 depletion only modestly affected pRPA and γH2AX levels (Figure 4E, compare lanes 4 & 5), RIF1 depletion caused increases in both markers (Figure 4E, compare lane 4 & 6), suggesting increased fork breakage in the absence of RIF1. To further examine this, we determined whether the increased fork breakage in the absence of RIF1 was modulated by SCAI and/or BRCA1. Co-depletion of SCAI and RIF1 did not further alter damage signaling at stalled forks (Figure S4E, lanes 4 & 5). However, loss of BRCA1 reduced signaling in the absence of RIF1 in the presence or absence of SCAI (Figure S4E, lanes 6 & 7). Finally, to determine whether this was a general function of RIF1 following replicative damage, we performed similar experiments as above (Figure S4E) following cisplatin treatment. In this context, and unlike what is seen following HU treatment, RIF1 depletion by itself had no effect on pRPA (Figure 4F, lane 4). Surprisingly, whereas 53BP1 depletion failed to restore resection in the absence of BRCA1 (Figure 4D, lane

7), loss of RIF1 fully restored resection upon cisplatin treatment in the absence of BRCA1 (Figure 4F, compare lanes 3 and 7) suggesting a possible antagonism between BRCA1 and RIF1 in this context. This phenotype was unique to RIF1 and was not shared by depletion of REV7, which mediates assembly of Shieldin complex members SHLD2 and SHLD3 [59, 62] (Figure S4F).

Loss of fork reversal at stalled forks confers a dependency on SCAI/REV3

We next wanted to determine at what step fork breakage occurs in the absence of SCAI/REV3. Our data so far suggests that BRCA1 drives DNA breakage at stalled forks upon replication stress. BRCA1 also has a well-established role in protecting arrested forks from degradation [63]. This difference in phenotypes may be due not only to the fact that forks keep progressing, albeit slowly, under our treatment conditions, but also that the forks may be processed differently by remodeling enzymes. The fork reversal activity of the enzymes SMARCAL1, ZRANB3 and HLTF represent a major mechanism of stalled fork processing [6, 7]. Multiple studies have shown that when forks progression is halted, fork reversal by these enzymes drives the creation of a chicken-foot structure that is protected from breakage and resection by BRCA1 [26, 27], a phenotype opposite to the BRCA1 activity we see under our conditions. We reasoned that if the fork breakage seen in the absence of SCAI was occurring downstream of fork reversal, it would be abolished upon depletion of fork reversal enzymes.

To determine whether fork reversal plays a similar role under our treatment conditions, we co-depleted SCAI and either SMARCAL1 or ZRANB3. To our surprise, rather than reduce fork breakage upon SCAI loss, knockdown of either SMARCAL1 or ZRANB3 led to consistent increases in pRPA and γH2AX upon HU treatment (Figure 5A, compare lanes 2, 5 & 8). The same phenotype was also seen upon co-depletion of REV3 and either SMARCAL1 or ZRANB3 (Figure 5A, compare lanes 3, 6 & 9). These results were further validated by knocking down SMARCAL1 with two independent siRNAs, which led to similar increases in the absence of SCAI (Figure 5B, compare lanes 2, 4 & 6). This phenotype was shared between SMARCAL1 and ZRANB3 and was seen with multiple siRNAs against SMARCAL1, suggested that not only was fork breakage in the absence of SCAI not occurring downstream of fork reversal, but that the process that leads to fork breakage might also compete with fork reversal for repair of stalled forks. An alternative explanation might be that fork breakage occurs downstream of a parallel fork reversal mechanism to that orchestrated by SMARCAL1/ZRANB3. Such a parallel mechanism has been suggested to occur via FBH1 [61]. To examine this, we knocked down FBH1 using siRNAs and observed that, similar to loss of SMARCAL1, FBH1 depletion also led to increased pRPA and γH2AX in the absence of SCAI (Figure 5C). Thus, depletion of multiple fork reversal enzymes all led to increased fork breakage in the absence of SCAI/REV3. The increased break formation in the absence of fork reversal was more marked in the absence of SCAI/REV3, which suggests that a SCAI/REV3-dependent mechanism might compete with fork reversal as a mechanism for stalled fork rescue.

RAD51 activity globally regulates stalled fork metabolism

RAD51 has been implicated in various fork processing roles in cells undergoing replication stress. It is important for fork reversal, protecting stalled forks against the

activity of nucleases, and is key for recombination through template switching [25]. RAD51's recombination function can be genetically uncoupled from the other functions, as multiple studies have shown that RAD51 strand exchange activity is not required for fork protection [61, 64, 65]. To determine if and how RAD51 regulates the phenotypes seen in the absence of SCAI/REV3, we first depleted RAD51 using a pool of siRNAs (Figure S5A). Depletion of RAD51 abolished the increased pRPA and γH2AX seen in the absence of SCAI (Figure S5A). We next tested RAD51's role using two independent siRNAs and observe similar effects – loss of RAD51 abolished pRPA and γH2AX upon HU treatment even when SCAI was absent (Figure 5D). To further determine how RAD51 contributes to the increased pRPA and γH2AX seen upon fork stalling, we tested the effect of inhibiting RAD51 strand exchange activity using a previously described inhibitor B02 [66]. Surprisingly, RAD51 inhibition completely abolished the signaling seen upon loss of SCAI or REV3 (Figure 5E, compare lanes 2&3 to lanes 5&6), without affecting cell cycle distribution (Figure S5B), suggesting that this function requires or occurs downstream of the strand exchange activity of RAD51. To directly test the effect on DNA break formation, we performed neutral comet assays. RAD51 depletion prevented DNA break formation in the absence of SCAI (Figure 5F).

We showed earlier that inhibition of fork reversal led to additive increases in fork breakage upon SCAI loss. We were curious whether this increase was also modulated by RAD51. Interestingly, RAD51 inhibition completely prevented the increased break signaling seen in the absence of SCAI when fork reversal was prevented either via SMARCAL1 knockdown (Figure 5G) or via PARP inhibition (Figure S5D) which has been shown to modulate fork reversal outcomes [15]. Taken together these data suggests that RAD51 strand exchange activity drives the formation of DNA breaks seen in the absence of SCAI/REV3, and that failure of fork reversal leads to increased RAD51 driven fork breakage when SCAI or REV3 is absent.

BRCA1-RAD51 axis governs SLX4 mediated fork breakage in the absence of SCAI

We next wanted to determine how fork breakage occurs in the absence of SCAI/REV3. Cells have several structure specific nucleases that orchestrate fork breakage [17]. In particular, MUS81 has been implicated in fork processing and restart under various conditions [67, 68]. We co-depleted SCAI or REV3 cells with siRNAs against SLX4 or MUS81 following treatment with HU. We found that loss of SLX4, but not MUS81, led to reduced γH2AX amounts in SCAI depleted cells (Figure 6A). A similar pattern was observed in REV3 depleted cells: MUS81 had no effect or led to moderate increases in γH2AX, while SLX4 loss reduced γH2AX levels (Figure 6B). To directly examine whether stalled fork breakage in the absence of SCAI was orchestrated by SLX4, we performed neutral comet assays. As expected, SCAI depletion led to increased comet tail moments which was significantly reduced by SLX4 depletion (Figure 6C).

We next sought to determine whether and how SLX4 was recruited to stalled forks and how this was modulated by loss of SCAI. Fractionation experiments revealed that SCAI loss led to increased amounts of SLX4 in the chromatin fraction compared to controls (Figure 6D, compare lanes 1 & 2). We did not observe such increases with other nucleases such as MUS81 or MRE11 (Figure 6D). Strikingly, RAD51 inhibition led to significant reduction in not only γH2AX levels, but also in the amount of SLX4 on

498 chromatin (Figure 6D), and the increased SLX4 amounts on chromatin seen in the
499 absence of SCAI was prevented by B02 treatment (Figure 6D, compare lanes 2 and 4).
500 Taken together, these experiments suggest that fork breakage in the absence of
501 SCAI/REV3 occurs downstream of RAD51 strand exchange activity but independent of
502 fork reversal.
503 To further characterize the mechanism by which stalled forks break, we depleted
504 BRCA1. Upon SCAI depletion, BRCA1 KO showed reduced chromatin levels of SLX4
505 compared to controls (Figure S6A); this finding is consistent with a prior report [24]. To
506 further examine this role, and to determine how it was modulated by RAD51, we
507 knocked down BRCA1 using siRNAs. HU treatment resulted in slightly increased
508 amounts of SLX4 on chromatin (Figure 6E, compare lanes 1 & 3). Similar to what was
509 seen following RAD51 inhibition or in BRCA1 KO cells, BRCA1 KD also resulted in
510 reduction in the amount of damage induced SLX4 on chromatin (Figure 6E, compare
511 lanes 1 & 3). Similar to what was seen following RAD51 inhibition or in BRCA1 KO cells,
512 BRCA1 KD also resulted in reduction in the amount of damage induced SLX4 on
513 chromatin (Figure 6E). Next, to determine how BRCA1 and RAD51 activities contributed
514 to fork breakage, we examined chromatin association of RAD51 and its modulation by
515 BRCA1. Upon treatment with HU, there was increased amounts of RAD51 on chromatin
516 (Figure 6E, compare lanes 1 & 3). Loss of BRCA1 significantly prevented the increase
517 in RAD51 amounts on chromatin (Figure 6E, lane 4). Next, we were curious to know
518 whether this effect of BRCA1 on RAD51 chromatin association could be modulated by
519 53BP1 loss under our conditions. Indeed, while BRCA1 loss almost completely
520 abolished RAD51 levels on chromatin (Figure 6F, compare lanes 1 & 2), co-depletion of
521 53BP1 partially restored the amount of RAD51 (compare lanes 2 and 4), suggesting
522 that the reduced RAD51 loading upon fork stalling was partly due to 53BP1 activity. This
523 effect was seen despite 53BP1 not affecting resection in our context (Figure 4D, 4E,
524 Figure S4D), and is consistent with recent results seen using CRISPR nickase
525 experiments [69] suggesting that 53BP1 antagonism of RAD51 loading is a general
526 effect of 53BP1 at broken forks. Taken together, our data show that the RAD51-BRCA1-
527 SLX4 axis drives break formation at stalled forks. BRCA1 controls RAD51 levels on
528 chromatin in this process and this can be counteracted by 53BP1.
529
530 **SCAI promotes genomic integrity and viability following replication fork stalling**
531 We have shown that SCAI loss leads to increased stalled fork breakage and
532 resection. We reasoned that unrepaired breaks in the absence of SCAI might persist
533 and contribute to genomic instability and cell death. To test this, we treated cells with
534 HU as before, then released from HU treatment and allowed cells to proceed into
535 mitosis (Figure 7A, top panel). We then performed mitotic DNA spreads to examine for
536 the presence of chromosomal abnormalities including breaks, gaps, fusions and similar
537 events. SCAI loss did not significantly impact the extent of chromosomal abnormalities
538 observed in the absence of HU treatment (Figure 7A). In contrast, following treatment
539 with HU, we observed that loss of SCAI led to significant increases in the amount of
540 broken and otherwise abnormal chromatids compared to control knockdown cells
541 (Figure 7A & B). To further examine SCAI's role, we performed colony formation assays.
542 SCAI depletion led to diminished viability upon treatment with HU (Figure 7C & D).
543 Taken together, these data show that SCAI is required for efficient repair and viability

following replication stress and that its loss results in persistence of unrepaired fork breakage that leads to heightened genomic instability.

DISCUSSION

In this work, we have uncovered a novel fork restoration mechanism requiring the activities of both the fork protecting factor SCAI and the DNA polymerase REV3 to prevent pathologic fork breakage upon replication stress. Our experiments reveal key roles for BRCA1 and RAD51, suggesting a homologous recombination mediated restart mechanism. Indeed, we find requirements for both the HR-promoting coiled-coil domain of BRCA1 as well as the strand exchange activity of RAD51. We propose that BRCA1-RAD51 drive break-independent fork restart that confers a dependency on the SCAI/REV3 complex (Figure 7E). Surprisingly, this process appears to occur either parallel to or upstream of SMARCAL1/ZRANB3 or FBH1-mediated fork reversal.

In addition to its canonical roles in regulating resection and consequent pathway choice at two-ended DSBs, BRCA1 has several proposed roles at stalled forks [70]. Its fork protection functions are well established, occurring downstream of fork reversal. Work in the literature has suggested roles for BRCA1 in stalled fork remodeling leading to fork restart [71]. Our experiments allow us to uncouple BRCA1's role from a fork protection function not only because BRCA1 loss paradoxically prevents fork breakage but also due to a requirement for BRCA1's coiled coil motif, which is dispensable for fork protection roles of BRCA1 [71]. Also, depletion of fork reversal factors, which are necessary to provide a substrate for fork protection, does not abolish the DNA break formation seen in the absence of SCAI but rather increases it. We also show that this role occurs independently of or distinct from BRCA1's known roles at two-ended DSBs: the C-terminus of BRCA1 is dispensable for promoting fork breakage and processing, and we directly rule out a role for BRCA1's resection partner, CtIP, in promoting break formation at stalled forks.

The 53BP1-Rif1 axis has been extensively studied in regulating two-ended replication-independent breaks, with several labs demonstrating resection and repair pathway choice control [72]. Because our system involves the generation of breaks at stalled forks via SLX4 activity, we have taken advantage of this as an opportunity to investigate in detail how fork breakage and resection at stalled forks is regulated by 53BP1-RIF1 axis. 53BP1 has been previously shown to protect stalled forks [61]; however, our SCAI-null context allows us to show here that 53BP1 does not influence DNA resection upon break formation at stalled forks. This was true whether forks were stalled by HU or at breaks resulting from cisplatin treatment. Rif1 has been shown to possess 53BP1 independent roles at forks [60]. It can be recruited to stalled forks in a 53BP1 independent manner, and here we show that RIF1 loss by itself led to increased fork breakage signaling. Whether this is related to Rif1's fork protection roles is not clear. We also observed what appeared to be an antagonism between BRCA1 and RIF1 in regulating resection upon ICL agent treatment. Removing BRCA1 enforced a RIF1-mediated block to resection. While 53BP1 did not affect stalled fork outcomes upon fork breakage, it seemed to modulate the extent of RAD51 amounts on chromatin. This is consistent with what was recently shown using CRISPR induced breakage [69].

We previously employed a Tus/Ter reporter to show that SCAI is particularly important for HR promotion at stalled forks [22]. Our results here suggest that this role is important for driving replication restart, and that this role occurs downstream of RAD51 activity. We hypothesize that certain regions of the genome are prone to stall the advancing replication fork and require SCAI and REV3 to direct fork restoration and repair. Indeed, using a fragile site reporter we found that SCAI/REV3 loss results in increased breaks [22], consistent with our current findings. While SCAI and REV3 appear to function in concert, they do not have overlapping roles, and loss of SCAI seemed to lead to a stronger restart defect than loss of REV3. Future work will uncover under what scenarios SCAI and REV3 function together and how REV3 is regulated differentially from its role in translesion synthesis.

A central role for RAD51 in promoting fork restart has been proposed by others [20], and the fork restart defects seen in the absence of SCAI appeared to occur downstream of RAD51 activity. BRCA1 depletion did not affect SCAI recruitment to chromatin, but results in significant reduction in RAD51 loading on chromatin. Our data suggests that the SCAI/REV3 mediated restart mechanism occurs in parallel with SMARCAL1 /ZRANB3 or FBH1 mediated fork reversal. Importantly, loss of fork reversal factors like SMARCAL1 paradoxically led to increased fork breakage in the absence of SCAI, suggesting that forks normally processed in a reversal mediated fashion are funneled into a SCAI dependent pathway that ultimately leads to fork breakage whenever SCAI was absent. Both pathways appear to require RAD51 activity, as inhibiting RAD51 prevented fork breakage whenever SCAI and SMARCAL1 were co-depleted. RAD51 has been proposed to cause a CMG helicase-containing bubble ahead of annealed parental strands [73]. RAD51 could promote restart by invading newly synthesized DNA ahead of the annealed fork. Under-replicated regions can then be duplicated by gap-synthesis post repair. BRCA1 is not essential for fork reversal [63], but may enhance RAD51 chromatin association to drive strand invasion mediated fork restart. We show that SCAI is required for fork restart in this context, and in the absence of SCAI, SLX4 accumulates on chromatin to cleave the resulting HR intermediates leading to fork breakage. Such broken forks can be engaged by alternative means of end joining or may persist leading to genomic instability and cell death. Whether the same RAD51 activity drives both reversal as well as HR-mediated fork restart will be a focus of future work.

626 **METHODS**
627 Cell lines
628 U2OS cells were originally obtained from ATCC (HTB-96). U2OS ΔSCAI and U2OS
629 cells expressing lentiCRISPR control gRNAs (WT) were previously described [22], and
630 were passaged in McCoy's 5A medium + L-Glutamine (16600-082, Gibco). hTERT-
631 RPE1 cells were originally obtained from ATCC (CRL-4000). All RPE1 cell lines and
632 their derivatives were passaged in DMEM/F12 (1:1) medium + L-Glutamine + 15mM
633 HEPES (11330-032, Gibco). RPE1 ΔBRCA1/Δp53 (referred to as ΔBRCA1 in Figure 3)
634 was a kind gift from Dr. Alan D'Andrea [74]. RPE1 TP53$^{-/-}$ GFP PINDUCER20 (referred
635 to as "parent" in Figures S4C and S6A), RPE1 TP53$^{-/-}$ BRCA1$^{-/-}$ GFP PINDUCER20
636 (referred to as "ΔBRCA1" in Figure 4A, 4B, S4C, and S6A), RPE1 Tp53$^{-/-}$ BRCA1$^{-/-}$
637 GFP-BRCA1 PINDUCER20 (referred to as "WT" in Figures 4A, 4B, 4C and "GFP-
638 BRCA1 Rescue" in Figure S4C) and RPE1 TP53$^{-/-}$ BRCA1$^{-/-}$ GFP-BRCA1 ΔCC
639 PINDUCER20 (referred to as ΔCC) were kind gifts from Dr. Andrew Blackford and were
640 previously described [48]. RPE1 Flag Cas9 TP53$^{-/-}$ ΔBRCA1 Δ53BP1 (referred to as
641 ΔBRCA1/Δ53BP1 in Figure S4D) were a kind gift from Dr. Dheva Setiaputra and were
642 previously described [59].
643
644 Reagents and Drugs
645 Dimethyl Sulfoxide (DMSO) was from Thomas Scientific (D0231). Hydroxyurea (HU)
646 was obtained from Sigma-Aldrich (H8627-5G). Aphidicolin (APH) was from Sigma-
647 Aldrich (A4487-1ML). The TLS inhibitor JH-RE-06 was obtained from MedChemExpress
648 (HY-126214, 10mM/1mLSolution). Cisplatin was from Selleck Chemicals (S1166-50mg).
649 Rad51 inhibitor B02 was from Sigma-Aldrich (553525-25MG). Olaparib from Selleck
650 Chemicals (S1060-25mg). Colcemid was obtained from Millipore Sigma (10295892001).
651
652 Antibodies
653 The antibodies used in this work include the following: Anti-vinculin 1:1000 (Sigma-
654 Aldrich, V9131-.2ML), vinculin (7F9) 1:200 (Santa Cruz Biotechnology, sc-73614), SCAI
655 1:500 (Abcam, ab124688), Chk1 (2G1D5) 1:1000 (Cell Signaling, 2360S), P-Chk1
656 (S345) (133D3) Rabbit mAb 1:1000 (Cell Signaling, 2348S), RPA 32 kDa subunit (9H8)
657 1:200 (Santa Cruz Biotechnology, sc-56770, only used for western blots), RPA32 1:200
658 (Genetex, GTX70258, only used for IF), Rabbit x-Phospho RPA32 (S4/S8) 1:1000
659 (Bethyl, A300-245A), H2AX 1:1000 (Bethyl, A300-082A), Anti-phospho-Histone H2A.X
660 (Ser139) 1:1000 (EMD Millipore Corp., 05-636), REV7 1:200 (Santa Cruz
661 Biotechnology, sc-135977), Anti-Exonuclease 1 (EXO1) 1:1000 (Bethyl, A302-640A),
662 ORC2 1:1000 (Abcam, ab68348), BRCA1 1:1000 (EMD Millipore Corp., 07-434), 53BP1
663 1:1000 (Bethyl, A300-272A), RIF1 1:1000 (Bethyl, A300-569A), CtIP 1:1000 (Bethyl,
664 A300-488A), SmarcAL1 (A-2) 1:200 (Santa Cruz Biotechnology, sc-376377), ZRANB3
665 1:1000 (Bethyl, A303-033A), FBH1 1:1000 (Abcam, ab58881), RAD51 1:1000 (Abcam,
666 ab63801), MUS81 1:200 (Santa Cruz Biotechnology, sc-53382), SLX4 1:1000 (Bethyl,
667 A302-270A), H3 1:1000 (Cell Signaling, 9715), MRE11 1:1000 (Abcam, ab214), Goat
668 anti-Mouse IgG (H+L) Secondary Antibody, HRP 1:2500 (Invitrogen, 31430), Goat anti-
669 Rabbit IgG (H+L) Secondary Antibody, HRP 1:2500 (Invitrogen, 31460), Goat anti-
670 Rabbit IgG (H+L) Highly Cross-Adsorbed Secondary Antibody, Alexa Fluor Plus 488
671 1:300 (Invitrogen, A32731), Goat anti-Mouse IgG (H+L) Highly Cross-Adsorbed

672 Secondary Antibody, Alexa Fluor Plus 594 1:300 (Invitrogen, A32742), Goat anti-Mouse
673 IgG (H+L) Highly Cross-Adsorbed Secondary Antibody, Alexa Fluor Plus 488 1:300
674 (Invitrogen, A32723).
675
676 siRNA transfections
677 RPE1 and U2OS cells were seeded onto 6-well plates and reverse transfected with 20-
678 40nM siRNA using Lipofectamine RNAiMAX reagent (13-778-150, Invitrogen) according
679 to the manufacturer's instructions. Cells were treated 48 h after treatment with drugs as
680 indicated in the legend and processed 16 to 18 h later.
681
682 SCAI rescue experiment
683 U2OS cells were transfected with plasmids using PolyJet reagent (SignaGen,
684 SL10068B) according to the manufacturer's instructions and treated with drugs as
685 indicated in the Figure legends. SCAI was cloned into the pcDNA3.1 backbone as
686 previously described [22]. The ORF sequence of SCAI was modified to avoid being
687 identified by gRNA in ΔSCAI cells. Specifically, GCTGAAGATGAT (Ala-Glu-Asp-Asp)
688 was replaced with GCAGAGGACGAC using a site-directed mutagenesis kit (New
689 England Biolabs, E0552S).
690
691 Western blotting
692 Cells were harvested, washed with ice cold phosphate-buffered saline (PBS), and lysed
693 in SDS lysis buffer (50 mM Tris HCl pH 6.8, 100 mM NaCl, 1.7% SDS, 10 mM NaF, 7%
694 glycerol) prior to sonication. Protein content was measured using Bradford reagent
695 (23236, Life Technologies) on an Eppendorf Biophotometer. Laemmli sample buffer
696 (1610747, Bio-Rad Laboratories) was added with 20 mM DTT prior to boiling the
697 samples for 5-10 min. Whole cell lysates were analyzed using sodium dodecyl sulfate
698 gel electrophoresis (SDS-PAGE) and transferred onto nitrocellulose membranes.
699 Membranes were blocked with 5% (wt/vol) milk in Tris-buffered saline with Tween
700 (TBST) for a minimum of 30 min and then probed with the indicated antibodies. Protein
701 bands were quantified with ImageJ.
702
703 Chromatin fractionation
704 Chromatin fractions were done as previously described [75]. Briefly, RPE1 cells
705 previously transfected with the indicated siRNAs were seeded into 10 cm plates, treated
706 with drugs as indicated, then harvested and washed with ice cold PBS. Sedimented
707 cells were resuspended in cold Solution 1 (10 mM Hepes (pH 7.9), 10 mM KCl, 1.5 mM
708 $MgCl_2$, 0.34 M sucrose, 1 mM DTT, 10% glycerol, 1mM Na_3VO_4, protease and
709 phosphatase inhibitors). Triton X-100 was added to 0.1%, and samples were incubated
710 on ice prior to centrifuging. The supernatant was removed as the cytoplasmic extract,
711 and sedimented nuclei were washed with Solution 1 prior to being lysed in Solution 2
712 (3 mM EDTA, 0.2 mM EGTA, 1 mM DTT, protease and phosphatase inhibitors) on ice.
713 Samples were centrifuged, washed with cold Solution 2, and then the chromatin-
714 enriched pellets were lysed with SDS lysis buffer. Chromatin extract samples were
715 sonicated, and protein content was measured. Sample buffer was added to all samples
716 and boiled prior to western blotting.
717

718 Cell cycle analyses
719 Cells were treated with indicated drugs for 18h prior to being harvested. Cells were then
720 washed with ice cold PBS, then fixed in 70% ethanol at 4 °C overnight. Samples were
721 pelleted, washed with ice cold PBS, and resuspended in 50 µg/mL propidium iodide
722 solution containing 0.1 mg/mL RNase A. Samples were then incubated at 37°C in the
723 dark for 15-30 min and flow cytometry was performed using a FACSymphony A5 (BD
724 Biosciences). Data were analyzed using FlowJo software.
725
726 Clonogenic survival assays
727 Cells were transfected as stated above for 48 h with the indicated siRNAs and then
728 treated with indicated doses of drugs for 18 h. The number of cells plated in six-well
729 plates was adjusted based on the dose of drug the cells were exposed to. Cells were
730 allowed to form colonies for 10-14 days prior to being fixed and stained using Crystal
731 Violet. Analyses were performed using ImageJ.
732
733 Immunofluorescence Assay
734 Cells were transfected with the indicated siRNAs as above and plated onto glass
735 coverslips 18 h later. 48 h after the transfection, the cells were treated with HU for the
736 indicated dose and duration. The cells were then washed with ice-cold PBS on ice, pre-
737 extracted for 5 min on ice using cytoskeleton buffer (100 mM NaCl, 10 mM HEPES (pH
738 7.8), 3 mM $MgCl_2$, 300 mM sucrose, 0.1% Triton X-100), fixed with 4%
739 paraformaldehyde in PBS for 10 min at room temp and then permeabilized with 0.5%
740 Triton-100 in 1X PBS. Samples were then blocked with 3% bovine serum albumin (BSA)
741 in PBS for a minimum of 30 min on a rocker followed by overnight incubation with
742 primary antibodies at 4 ^{o}C in a humidified chamber. Unbound primary antibodies were
743 washed using 3% BSA in PBS and then samples incubated with secondary antibody for
744 1 h at RT in the dark. Unbound antibody was washed with PBS and then samples
745 stained with 1 µg/ml DAPI for 1 h before mounting the coverslips on a microscope slide
746 for imaging. Images were acquired using an LSM 780 NLO (Zeiss), and a minimum of
747 100 nuclei for each group were analyzed using ImageJ.
748
749 QIBC image acquisition and analysis
750 Fixed and stained slides were imaged on a Molecular Devices ImageXpress Microscope
751 equipped with a Nikon 40x/0.95 PlanApo objective. Around 2000 nuclei were acquired
752 for each condition. Quantification was then performed using the "Multi Wavelength Cell
753 Scoring" module in the MetaXpress software. Briefly, nuclei were segmented using the
754 DAPI channel, and the raw Mean Fluorescent Intensities (MFIs) of each nucleus were
755 measured for DAPI, RPA (AF488), and gamma-H2AX (AF594). All cells were then
756 plotted for each condition and p-values generated by Ordinary one-way ANOVA,
757 Tukey's multiple comparison test
758
759 DNA fiber assays
760 hTERT-RPE1 cells were reverse transfected with the indicated siRNAs at 20 nM using
761 Lipofectamine RNAiMAX reagent (Invitrogen). Transfected hTERT-RPE1 cells were
762 pulse-labeled with CldU followed by IdU as indicated in each Figure. After being labeled,
763 cells were harvested and embedded in 0.6% low melting point agarose gel plugs. Cells

764 in plugs were incubated with lysis solution (0.2 M EDTA, 0.5% SDS, 3 mg/mL
765 Proteinase K) overnight at 50°C. Each plug was dissolved in 0.5 M MES solution (pH
766 5.5) by β-agarase (NEB) overnight treatment and DNA was attached to a pre-treated
767 coverslip (PolyAn) using FiberComb® Molecular Combing System (GENOMIC VISION).
768 DNA on coverslips was denatured by incubating in denaturing solution (0.5 N NaOH, 1
769 M NaCl) for 8 min. Blocking was performed with 5% BSA in PBS for 60 min. For
770 immunostaining, coverslips were incubated overnight with primary antibodies; ab6326
771 anti-BrdU (cross-reacts with CldU) antibody (rat) (1:50) and BD Biosciences 347580
772 anti-BrdU (cross-reacts with IdU) antibody (mouse) (1:8). Slides were washed with PBS
773 followed by incubation for one hour with the secondary antibodies; anti-rat Alexa-488
774 antibody (1:300) and anti-mouse Alexa-594 antibody (1:300). After wash with PBS,
775 coverslips were mounted onto glass slides with anti-fade mounting medium
776 (SlowFade™ Glass Soft-Set Antifade Mountant, Invitrogen). Images were acquired with
777 Leica STELLARIS confocal microscope. DNA fiber numbers and lengths were manually
778 analyzed using LAS X software (Leica Microsystems).
779
780 Metaphase spreads
781 hTERT-RPE1 cells were reverse transfected with the indicated siRNAs as above using
782 Lipofectamine RNAiMAX. Two days after the transfection, cells were treated with 2 mM
783 HU or PBS for 18 h, followed by PBS wash and 24 h incubation in normal medium.
784 Cells were exposed to colcemid (100 ng/ml) for the last 3 h of the 24 h normal medium
785 incubation before harvest. Collected cells were treated with a hypotonic solution (1:2
786 mixture of 0.075 M KCl and 0.9% Na citrate) for 10 min and fixed with 3:1 methanol:
787 acetic acid. Fixed cells were transferred on glass slides dropwise, and the slides were
788 stained with Giemsa stain. Cells in metaphase were observed using a Zeiss Axiovert
789 200M microscope and captured using AxioVision. Over 50 metaphase cells were
790 analyzed per sample.
791
792 Neutral Comet assay
793 hTERT-RPE1 cells were reverse transfected with the indicated siRNAs at 20 nM using
794 Lipofectamine RNAiMAX reagent (Invitrogen). Two days after the transfection, cells
795 were treated with 2 mM HU or PBS for 40 h. After HU treatment, cells were harvested
796 and resuspended in ice-cold PBS. 10µL of the cell suspension was mixed with 100 µL of
797 melted 0.7% low melting point agarose gel, and the mixture was spread onto a pre-
798 coated CometSlide™ (R&D SYSTEMS®). After the agarose gel was solidified at 4 °C,
799 the slide was immersed in lysis solution (10 mM Tris base, 2.5 M NaCl, 100 mM Na_2-
800 EDTA, 10% DMSO, 1% Triton X-100, pH 10) for 2 h at 4 °C followed by a 30 min
801 incubation in neutral electrophoresis buffer (100 mM Tris base, 300 mM sodium acetate,
802 pH 9). Then, the slide was placed in an electric field for 40 min. After the
803 electrophoresis, the slide was immersed in DNA precipitation solution (82% ethanol, 1
804 mM ammonium acetate) for 30 min followed by a 30 min incubation in 70% ethanol.
805 SYBR Gold dye (Invitrogen) was used to stain DNA ("comet") and images were
806 obtained with TissueFAXS (TissueGnostics). Comets were analyzed with ImageJ
807 (OpenComet).
808
809 Quantification and statistical analyses

Statistical analyses were performed using Prism 10 (GraphPad). All statistics used are indicated in the Figure legends. For all experiments: n.s. $P \geq 0.05$; *$P<0.05$; **$P < 0.01$; ***$P < 0.001$; ****$P<0.0001$. All experiments in this work were performed multiple independent times with similar results. Multiple siRNAs, multiple knockout clones, and multiple cell lines were analyzed to confirm that results were not caused by off-target effects or clonal variations. Representative images and/or experiments are shown for westerns, cell cycle analyses, DNA fiber assays and IFs.

REFERENCES AND NOTES

1. Zeman, M.K. and K.A. Cimprich, *Causes and consequences of replication stress.* Nat Cell Biol, 2014. **16**(1): p. 2-9.
2. Ciccia, A. and S.J. Elledge, *The DNA damage response: making it safe to play with knives.* Mol Cell, 2010. **40**(2): p. 179-204.
3. Saxena, S. and L. Zou, *Hallmarks of DNA replication stress.* Mol Cell, 2022. **82**(12): p. 2298-2314.
4. Gaillard, H., T. Garcia-Muse, and A. Aguilera, *Replication stress and cancer.* Nat Rev Cancer, 2015. **15**(5): p. 276-89.
5. Cimprich, K.A. and D. Cortez, *ATR: an essential regulator of genome integrity.* Nat Rev Mol Cell Biol, 2008. **9**(8): p. 616-27.
6. Neelsen, K.J. and M. Lopes, *Replication fork reversal in eukaryotes: from dead end to dynamic response.* Nat Rev Mol Cell Biol, 2015. **16**(4): p. 207-20.
7. Quinet, A., D. Lemacon, and A. Vindigni, *Replication Fork Reversal: Players and Guardians.* Mol Cell, 2017. **68**(5): p. 830-833.
8. Schlacher, K., et al., *Double-strand break repair-independent role for BRCA2 in blocking stalled replication fork degradation by MRE11.* Cell, 2011. **145**(4): p. 529-42.
9. Errico, A. and V. Costanzo, *Mechanisms of replication fork protection: a safeguard for genome stability.* Crit Rev Biochem Mol Biol, 2012. **47**(3): p. 222-35.
10. Petermann, E. and T. Helleday, *Pathways of mammalian replication fork restart.* Nat Rev Mol Cell Biol, 2010. **11**(10): p. 683-7.
11. Scully, R., et al., *Recombination and restart at blocked replication forks.* Curr Opin Genet Dev, 2021. **71**: p. 154-162.
12. Zellweger, R., et al., *Rad51-mediated replication fork reversal is a global response to genotoxic treatments in human cells.* J Cell Biol, 2015. **208**(5): p. 563-79.
13. Petermann, E., et al., *Hydroxyurea-stalled replication forks become progressively inactivated and require two different RAD51-mediated pathways for restart and repair.* Mol Cell, 2010. **37**(4): p. 492-502.
14. Mouron, S., et al., *Repriming of DNA synthesis at stalled replication forks by human PrimPol.* Nat Struct Mol Biol, 2013. **20**(12): p. 1383-9.
15. Berti, M., et al., *Human RECQ1 promotes restart of replication forks reversed by DNA topoisomerase I inhibition.* Nat Struct Mol Biol, 2013. **20**(3): p. 347-54.
16. Pepe, A. and S.C. West, *MUS81-EME2 promotes replication fork restart.* Cell Rep, 2014. **7**(4): p. 1048-55.
17. Sarbajna, S., D. Davies, and S.C. West, *Roles of SLX1-SLX4, MUS81-EME1, and GEN1 in avoiding genome instability and mitotic catastrophe.* Genes Dev, 2014. **28**(10): p. 1124-36.
18. Kockler, Z.W., et al., *Repair of DNA Breaks by Break-Induced Replication.* Annu Rev Biochem, 2021. **90**: p. 165-191.
19. Kramara, J., B. Osia, and A. Malkova, *Break-Induced Replication: The Where, The Why, and The How.* Trends Genet, 2018. **34**(7): p. 518-531.

20. Ait Saada, A., S.A.E. Lambert, and A.M. Carr, *Preserving replication fork integrity and competence via the homologous recombination pathway.* DNA Repair (Amst), 2018. **71**: p. 135-147.
21. Chakraborty, S., K. Schirmeisen, and S.A. Lambert, *The multifaceted functions of homologous recombination in dealing with replication-associated DNA damages.* DNA Repair (Amst), 2023. **129**: p. 103548.
22. Adeyemi, R.O., et al., *The Protexin complex counters resection on stalled forks to promote homologous recombination and crosslink repair.* Mol Cell, 2021. **81**(21): p. 4440-4456 e7.
23. Lemay, J.F., et al., *A genome-wide screen identifies SCAI as a modulator of the UV-induced replicative stress response.* PLoS Biol, 2022. **20**(10): p. e3001543.
24. Xu, Y., et al., *53BP1 and BRCA1 control pathway choice for stalled replication restart.* Elife, 2017. **6**.
25. Bhat, K.P. and D. Cortez, *RPA and RAD51: fork reversal, fork protection, and genome stability.* Nat Struct Mol Biol, 2018. **25**(6): p. 446-453.
26. Kolinjivadi, A.M., et al., *Smarcal1-Mediated Fork Reversal Triggers Mre11-Dependent Degradation of Nascent DNA in the Absence of Brca2 and Stable Rad51 Nucleofilaments.* Mol Cell, 2017. **67**(5): p. 867-881 e7.
27. Vujanovic, M., et al., *Replication Fork Slowing and Reversal upon DNA Damage Require PCNA Polyubiquitination and ZRANB3 DNA Translocase Activity.* Mol Cell, 2017. **67**(5): p. 882-890 e5.
28. Berti, M., D. Cortez, and M. Lopes, *The plasticity of DNA replication forks in response to clinically relevant genotoxic stress.* Nat Rev Mol Cell Biol, 2020. **21**(10): p. 633-651.
29. Cortez, D., *Preventing replication fork collapse to maintain genome integrity.* DNA Repair (Amst), 2015. **32**: p. 149-157.
30. Dungrawala, H., et al., *The Replication Checkpoint Prevents Two Types of Fork Collapse without Regulating Replisome Stability.* Mol Cell, 2015. **59**(6): p. 998-1010.
31. Sirbu, B.M., et al., *Analysis of protein dynamics at active, stalled, and collapsed replication forks.* Genes Dev, 2011. **25**(12): p. 1320-7.
32. Toledo, L.I., et al., *ATR prohibits replication catastrophe by preventing global exhaustion of RPA.* Cell, 2013. **155**(5): p. 1088-103.
33. Ikegami, S., et al., *Aphidicolin prevents mitotic cell division by interfering with the activity of DNA polymerase-alpha.* Nature, 1978. **275**(5679): p. 458-60.
34. Macheret, M. and T.D. Halazonetis, *DNA replication stress as a hallmark of cancer.* Annu Rev Pathol, 2015. **10**: p. 425-48.
35. Zhao, L. and M.T. Washington, *Translesion Synthesis: Insights into the Selection and Switching of DNA Polymerases.* Genes (Basel), 2017. **8**(1).
36. Wojtaszek, J.L., et al., *A Small Molecule Targeting Mutagenic Translesion Synthesis Improves Chemotherapy.* Cell, 2019. **178**(1): p. 152-159 e11.
37. Byun, T.S., et al., *Functional uncoupling of MCM helicase and DNA polymerase activities activates the ATR-dependent checkpoint.* Genes Dev, 2005. **19**(9): p. 1040-52.
38. Densham, R.M. and J.R. Morris, *Moving Mountains-The BRCA1 Promotion of DNA Resection.* Front Mol Biosci, 2019. **6**: p. 79.

39. Tarsounas, M. and P. Sung, *The antitumorigenic roles of BRCA1-BARD1 in DNA repair and replication.* Nat Rev Mol Cell Biol, 2020. **21**(5): p. 284-299.
40. Baer, R. and T. Ludwig, *The BRCA1/BARD1 heterodimer, a tumor suppressor complex with ubiquitin E3 ligase activity.* Curr Opin Genet Dev, 2002. **12**(1): p. 86-91.
41. Hansen, R.K., et al., *SCAI promotes DNA double-strand break repair in distinct chromosomal contexts.* Nat Cell Biol, 2016. **18**(12): p. 1357-1366.
42. Rickman, K.A., et al., *Distinct roles of BRCA2 in replication fork protection in response to hydroxyurea and DNA interstrand cross-links.* Genes Dev, 2020. **34**(11-12): p. 832-846.
43. Savage, K.I. and D.P. Harkin, *BRCA1, a 'complex' protein involved in the maintenance of genomic stability.* FEBS J, 2015. **282**(4): p. 630-46.
44. Wang, B., et al., *Abraxas and RAP80 form a BRCA1 protein complex required for the DNA damage response.* Science, 2007. **316**(5828): p. 1194-8.
45. Cruz-Garcia, A., A. Lopez-Saavedra, and P. Huertas, *BRCA1 accelerates CtIP-mediated DNA-end resection.* Cell Rep, 2014. **9**(2): p. 451-9.
46. Yun, M.H. and K. Hiom, *CtIP-BRCA1 modulates the choice of DNA double-strand-break repair pathway throughout the cell cycle.* Nature, 2009. **459**(7245): p. 460-3.
47. Wu, X. and B. Wang, *Abraxas suppresses DNA end resection and limits break-induced replication by controlling SLX4/MUS81 chromatin loading in response to TOP1 inhibitor-induced DNA damage.* Nat Commun, 2021. **12**(1): p. 4373.
48. Tsukada, K., et al., *BLM and BRCA1-BARD1 coordinate complementary mechanisms of joint DNA molecule resolution.* Mol Cell, 2024. **84**(4): p. 640-658 e10.
49. Ceppi, I., et al., *Mechanism of BRCA1-BARD1 function in DNA end resection and DNA protection.* Nature, 2024. **634**(8033): p. 492-500.
50. Bunting, S.F., et al., *53BP1 inhibits homologous recombination in Brca1-deficient cells by blocking resection of DNA breaks.* Cell, 2010. **141**(2): p. 243-54.
51. Hustedt, N. and D. Durocher, *The control of DNA repair by the cell cycle.* Nat Cell Biol, 2016. **19**(1): p. 1-9.
52. Nakamura, K., et al., *H4K20me0 recognition by BRCA1-BARD1 directs homologous recombination to sister chromatids.* Nat Cell Biol, 2019. **21**(3): p. 311-318.
53. Becker, J.R., et al., *BARD1 reads H2A lysine 15 ubiquitination to direct homologous recombination.* Nature, 2021. **596**(7872): p. 433-437.
54. Escribano-Diaz, C., et al., *A cell cycle-dependent regulatory circuit composed of 53BP1-RIF1 and BRCA1-CtIP controls DNA repair pathway choice.* Mol Cell, 2013. **49**(5): p. 872-83.
55. Jaspers, J.E., et al., *Loss of 53BP1 causes PARP inhibitor resistance in Brca1-mutated mouse mammary tumors.* Cancer Discov, 2013. **3**(1): p. 68-81.
56. Isobe, S.Y., et al., *Inhibition of RIF1 by SCAI Allows BRCA1-Mediated Repair.* Cell Rep, 2017. **20**(2): p. 297-307.
57. Scully, R., J.C. Walter, and A. Nussenzweig, *One-ended and two-ended breaks at nickase-broken replication forks.* DNA Repair (Amst), 2024. **144**: p. 103783.

58. Dev, H., et al., *Shieldin complex promotes DNA end-joining and counters homologous recombination in BRCA1-null cells.* Nat Cell Biol, 2018. **20**(8): p. 954-965.
59. Noordermeer, S.M., et al., *The shieldin complex mediates 53BP1-dependent DNA repair.* Nature, 2018. **560**(7716): p. 117-121.
60. Mukherjee, C., et al., *RIF1 promotes replication fork protection and efficient restart to maintain genome stability.* Nat Commun, 2019. **10**(1): p. 3287.
61. Liu, W., et al., *Two replication fork remodeling pathways generate nuclease substrates for distinct fork protection factors.* Sci Adv, 2020. **6**(46).
62. Liang, L., et al., *Molecular basis for assembly of the shieldin complex and its implications for NHEJ.* Nat Commun, 2020. **11**(1): p. 1972.
63. Taglialatela, A., et al., *Restoration of Replication Fork Stability in BRCA1- and BRCA2-Deficient Cells by Inactivation of SNF2-Family Fork Remodelers.* Mol Cell, 2017. **68**(2): p. 414-430 e8.
64. Mason, J.M., et al., *Non-enzymatic roles of human RAD51 at stalled replication forks.* Nat Commun, 2019. **10**(1): p. 4410.
65. Halder, S., et al., *Double-stranded DNA binding function of RAD51 in DNA protection and its regulation by BRCA2.* Mol Cell, 2022. **82**(19): p. 3553-3565 e5.
66. Huang, F., et al., *Identification of specific inhibitors of human RAD51 recombinase using high-throughput screening.* ACS Chem Biol, 2011. **6**(6): p. 628-35.
67. Lai, X., et al., *MUS81 nuclease activity is essential for replication stress tolerance and chromosome segregation in BRCA2-deficient cells.* Nat Commun, 2017. **8**: p. 15983.
68. Mayle, R., et al., *DNA REPAIR. Mus81 and converging forks limit the mutagenicity of replication fork breakage.* Science, 2015. **349**(6249): p. 742-7.
69. Pavani, R., et al., *Structure and repair of replication-coupled DNA breaks.* Science, 2024. **385**(6710): p. eado3867.
70. Rickman, K. and A. Smogorzewska, *Advances in understanding DNA processing and protection at stalled replication forks.* J Cell Biol, 2019. **218**(4): p. 1096-1107.
71. Daza-Martin, M., et al., *Isomerization of BRCA1-BARD1 promotes replication fork protection.* Nature, 2019. **571**(7766): p. 521-527.
72. Scully, R., et al., *DNA double-strand break repair-pathway choice in somatic mammalian cells.* Nat Rev Mol Cell Biol, 2019. **20**(11): p. 698-714.
73. Liu, W., et al., *RAD51 bypasses the CMG helicase to promote replication fork reversal.* Science, 2023. **380**(6643): p. 382-387.
74. Lim, K.S., et al., *USP1 Is Required for Replication Fork Protection in BRCA1-Deficient Tumors.* Mol Cell, 2018. **72**(6): p. 925-941 e4.
75. Tischler, J.D., et al., *FLIP(C1orf112)-FIGURENL1 complex regulates RAD51 chromatin association to promote viability after replication stress.* Nat Commun, 2024. **15**(1): p. 866.

Acknowledgements
We thank all the members of the Adeyemi laboratory for advice and helpful discussions. We thank Dr. Blackford and Dr. Setiaputra for providing reagents.

Funding
This work was supported by NIH NIGMS R35 GM150532-01 and an Early Career Investigator Grant from the Ovarian Cancer Research Alliance (ECIG-2023-3-1004) (to ROA). R.B. was supported by a Washington Research Foundation fellowship. This research was also supported by the Cellular Imaging Shared Resource RRID:SCR_022609 and the Flow Cytometry Shared Resource, RRID:SCR_022613, of the Fred Hutch / University of Washington / Seattle Children's Cancer Consortium (P30 CA015704).

Author Contributions
Conceptualization: R.O.A., Methodology: C.U., H.T., R.B., X.J., R.O.A., Investigation: C.U., H.T., R.B., X.J., R.O.A., Visualization: C.U., H.T., R.B., X.J., S.K., R.O.A., Supervision: R.O.A., Writing—original draft: R.O.A., Writing—review & editing: C.U., H.T., R.B., X.J., S.K., R.O.A.

Competing Interests
The authors declare that they have no competing interests.

Data and Materials Availability
All data needed to evaluate the conclusions in the paper are present in the paper and/or the Supplementary Materials. Materials resulting from the findings of this study are available from the corresponding author upon request.

1025 **MAIN FIGURE LEGENDS**
1026
1027 **Figure 1**. **SCAI promotes integrity and efficient restart of stalled replication forks**.
1028 **A**. Schematic of pulse-labeling DNA strands, representative images and lengths of two-
1029 color DNA fibers. DNA fibers were from hTERT-RPE1 cells transfected with siRNAs as
1030 indicated. **B**. Schematic of pulse-labeling DNA strands, representative images and
1031 lengths of single- and two-color DNA fibers. The top two panels indicate duel-labelled
1032 conditions, while the lower panels indicate single labelled conditions. DNA fibers were
1033 from hTERT-RPE1 cells transfected with siRNAs as indicated. **C**. Schematic of pulse-
1034 labeling DNA strands, representative images and lengths of two-color DNA fibers. DNA
1035 fibers were from hTERT-RPE1 cells transfected with siRNAs as indicated. **A**–**C**, red line
1036 represents median, three independent experiments, representative experiment shown.
1037 Mann Whitney test for two group comparison and Kruskal-Wallis followed by Dunn's
1038 multiple comparison test for more than three group comparison. ns – not significant ($P \geq$
1039 0.05).
1040
1041 **Figure 2. SCAI/REV3 limits breakage of stalled replication forks.**
1042 **A.** WT RPE1 cells transfected with the indicated siRNAs for 60 h, then treated with 2
1043 mM hydroxyurea (HU) for 18 h, harvested, and processed for western blotting with the
1044 specified antibodies. ND, no drug. **B.** Western blots (WB) from WT and SCAI-null U2OS
1045 cell lines treated with 1 mM HU for 18 h. **C.** WT and ΔSCAI U2OS cells were transfected
1046 with either backbone plasmids (Vector) or plasmids expressing SCAI that is resistant to
1047 CRISPR/Cas9 editing. After 30 h, cells were treated with 1.5 mM HU for another 18 h
1048 before immunoblotting. **D.** WT RPE1 cells were transfected with the indicated siRNAs,
1049 then treated with vehicle (DMSO), 1 μM, or 2 μM aphidicolin (APH) for 18 h before
1050 being processed for western blotting with the specified antibodies. **E-F**. Comet assay of
1051 hTERT-RPE1 (**E**) and U2OS (**F**) cells treated with 2 mM HU for 40 h. Indicated siRNAs
1052 were transfected two days before HU treatment. Red line represents median, three
1053 independent experiments, representative experiment shown. Kruskal-Wallis followed by
1054 Dunn's multiple comparison test. **G.** WT RPE1 cells were transfected with the indicated
1055 siRNAs, then treated with 1 mM HU for 18 h and assayed for the indicated proteins by
1056 WB. γH2AX values are normalized to vinculin loading control. **H-J**. Representative
1057 microscopy images showing chromatin bound RPA and γH2AX, following transient
1058 knockdown of SCAI or REV3 and 16 h treatment with 1.5 mM HU in hTERT RPE1
1059 wildtype cells (e) scale bar indicates 25 micron. Quantification of the integrated
1060 fluorescent intensity of RPA (f) and γH2AX (g) of cells in e, red bar indicates mean and
1061 SEM of about 2000 nuclei. ****$p < 0.0001$, Tukey's test.
1062
1063 **Figure 3. BRCA1 promotes increased fork breakage and resection in the absence**
1064 **of SCAI/REV3.**
1065 **A.** WT and BRCA1 null RPE1 cells were transfected with the indicated siRNAs, then
1066 treated with 1 mM HU for 18 h prior to blotting for the indicated proteins. **B.** WT and
1067 BRCA1-null RPE1 cells were transfected with the indicated siRNAs. Cells were then
1068 treated with 1 mM HU for 18 h before WCLs (whole cell lysates) were prepared and WB
1069 were performed against the indicated proteins. **C.** IF images showing RPA foci in WT
1070 RPE1 cells following treatment with the indicated siRNAs. Cells were treated with 1.5

1071 mM HU for 18 h prior to IF. Scale bars indicate 5 microns. **D.** Quantification of (**C**). ****P
1072 < 0.0001, unpaired Welch's t test (two-tailed). **E.** IF analyses showing representative
1073 γH2AX foci in WT and BRCA1-null RPE1 cells post-treatment with indicated siRNAs.
1074 Cells were treated with 1.5 mM HU for 18 h prior to IF analyses. Scale bars indicate 5
1075 microns. **F**. Quantification of (**E**). *P = 0.0337, unpaired Welch's t test (two-tailed). **G**.
1076 Comet assay of hTERT-RPE1 cells treated with 2 mM HU for 40 h. Indicated siRNAs
1077 were transfected two days before HU treatment. Red line represents median, two
1078 independent experiments, representative experiment shown. Kruskal-Wallis followed by
1079 Dunn's multiple comparison test. ns – not significant (P ≥ 0.05). **H.** WT and BRCA1-null
1080 RPE1 cells were transfected with the indicated siRNAs, then treated with 1 mM HU for
1081 18 h and fractioned prior to blotting for the indicated proteins. CE – cytoplasmic extract.
1082 SCAI values are normalized to ORC2 loading control.
1083
1084 **Figure 4. BRCA1 pro-breakage / resection roles at stalled and broken forks occur**
1085 **independently of 53BP1 but is modulated by Rif1.**
1086 **A.** GFP-WT-BRCA1 rescue (labeled WT), BRCA1-null (Δ), and GFP-BRCA1-S1655
1087 (S1655) RPE1 cells were transfected with the indicated siRNAs, then treated with 2 mM
1088 HU for 18 h. WCLs were assayed for the indicated proteins by WB. **B.** GFP-WT-BRCA1
1089 rescue (WT), BRCA1-null (Δ), and GFP-BRCA1-ΔCC (ΔCC) RPE1 cells were
1090 transfected with the indicated siRNAs, then treated with 2 mM HU for 18 h and assayed
1091 for the indicated proteins by WB. **C.** Western blots from GFP-WT-BRCA1 rescue (WT),
1092 and GFP-BRCA1-ΔCC (ΔCC) RPE1 cell lines transfected with the indicated siRNAs and
1093 treated with ND, 0.75 mM (Lanes 4-5), 1.5 mM (Lanes 6-7), or 3 mM (Lanes 8-9) HU for
1094 18 h. **D.** Western blots from WT and SCAI-null U2OS cells transfected with the indicated
1095 siRNAs and then treated with 2 μM cisplatin for 18 h. **E.** WT U2OS cells were
1096 transfected with the indicated siRNAs, then treated with 1 mM HU for 18 h and assayed
1097 for the indicated proteins by WB. **F.** WT and SCAI-null U2OS cells were transfected with
1098 the indicated siRNAs, then treated with 1.5 μM cisplatin for 18 h. Whole cell lysates
1099 were prepared, and WB were performed against the indicated proteins.
1100
1101 **Figure 5. Loss of fork reversal at Stalled Forks confers increased RAD51-**
1102 **depedent fork breakage in the absence of SCAI/REV3.**
1103 **A.** Western blots from WT RPE cells transfected with the indicated siRNAs and then
1104 treated with 1 mM HU for 18 h. **B.** WT RPE1 cells were transfected with the indicated
1105 siRNAs, then treated with 1 mM HU for 18 h and assayed for the indicated proteins by
1106 WB. **C.** WT RPE1 cells were transfected for and treated with 1 mM HU for 18 h. WCLs
1107 were prepared, and WB were performed against the indicated proteins. **D.** Western
1108 blots from WT RPE cells transfected with the indicated siRNAs and then treated with 2
1109 mM HU for 18 h. **E.** Western blots against the indicated proteins from WT RPE1 cells
1110 transfected, then pretreated with 27 μM RAD51 inhibitor B02 or vehicle (DMSO) for 30
1111 min and treated with 1 mM HU for 18 h. **F**. Comet assay of hTERT-RPE1 cells treated
1112 with 2 mM HU for 40 h. Indicated siRNAs were transfected two days before HU
1113 treatment. Red line represents median, three independent experiments, representative
1114 experiment shown. Mann Whitney test. **G.** Western blots from WT RPE cells transfected
1115 with the indicated siRNAs, pretreated with 27 μM RAD51 inhibitor B02 or vehicle
1116 (DMSO) for 30 min, then treated with 1 mM HU for 18 h.

1117
1118
1119
1120 **Figure 6. BRCA1-RAD51 axis governs SLX4 mediated fork breakage in the**
1121 **absence of SCAI.**
1122 **A.** WT RPE1 cells were transfected and treated with 2 mM HU for 18 h. WCLs were
1123 prepared, and WB were performed against the indicated proteins. **B.** Western blots from
1124 WT RPE cells transfected with the indicated siRNAs and then treated with 1 mM HU for
1125 18 h. **C**. Comet assay of hTERT-RPE1 cells treated with 2 mM HU for 40 h. Indicated
1126 siRNAs were transfected two days before HU treatment. Red line represents median,
1127 three independent experiments, representative experiment shown. Kruskal-Wallis
1128 followed by Dunn's multiple comparison test. ns – not significant ($P \geq 0.05$). **D.** WT
1129 RPE1 cells were transfected with the indicated siRNAs, then treated with 1.5 mM HU for
1130 18 h and fractioned prior to blotting for the indicated proteins. SLX4 values are
1131 normalized to ORC2 loading control. **E.** WT RPE1 cells were transfected and then
1132 treated with 2 mM HU for 18 h. Samples were processed for chromatin fraction prior to
1133 blotting for the indicated proteins. **F.** WT RPE1 cells were transfected with the indicated
1134 siRNAs, then treated with 2 mM HU for 18 h and fractioned prior to blotting for the
1135 indicated proteins.
1136
1137 **Figure 7. SCAI loss leads to increased genomic instability and cell death**
1138 **following replication stress.**
1139 **A**. Schematic of cell treatment protocol and numbers of chromosomal aberrations per
1140 metaphase cell. hTERT-RPE1 cells treated with 2 mM HU for 18h followed by washout
1141 of HU and 24 h incubation in normal medium. Indicated siRNAs were transfected two
1142 days before HU treatment. Three independent experiments, mean ± S.D. Ordinary one-
1143 way ANOVA followed by Tukey's multiple comparison test. ns – not significant ($P \geq$
1144 0.05). **B**. Representative images of A. Red arrow – chromosomal aberrations. **C.** WT
1145 RPE1 cells were transfected, then treated with the indicated doses of HU for 18 h and
1146 allowed to form colonies. Mean ± SD shown. **D.** Representative images from (C) are
1147 shown. **E.** Working model showing proposed roles of BRCA1, RAD51 and SCAI/REV3
1148 upon fork stalling.
1149

1150 **SUPPLEMENTARY FIGURE LEGENDS**
1151 **Figure S1**.
1152 **A**. Top. Schematic of pulse-labeling DNA strands, percentage of single- and two-color
1153 fibers and lengths of fibers. DNA fibers were from hTERT-RPE1 cells transfected with
1154 siRNAs as indicated.
1155
1156 **Figure S2.**
1157 **A.** WT RPE1 cells were transfected with the indicated siRNAs and then treated with 2
1158 mM HU for the indicated times. WB were performed against the indicated proteins. **B.**
1159 Western blots against the indicated proteins from WT RPE1 cells pretreated with 10 μM
1160 TLS inhibitor JH-RE-06 or vehicle (DMSO) for 30 min, then treated with 1.5 mM HU for
1161 18 h. **C.** WT and SCAI-null U2OS cells were treated with the indicated siRNAs, then
1162 treated with 1mM HU for 18 h prior to blotting for the indicated proteins**. D.** IF analyses
1163 showing representative RPA foci (left panel) in WT RPE1 cells post-treatment with
1164 indicated siRNAs. Cells were treated with 1 mM HU for 18 h prior to IF. Merge includes
1165 γH2AX foci and DAPI. Scale bars indicate 5 microns. Intensity of nuclear γH2AX
1166 staining was quantified using ImageJ and plotted on the right. ****P < 0.0001, Analysis
1167 of Variance (ANOVA). **E.** Left, representative immunofluorescence (IF) images showing
1168 γH2AX foci in WT RPE1 cells following treatment with the indicated siRNAs. Cells were
1169 treated with 1.5 mM HU for 18 h prior to IF analyses. Scale bars indicate 5 microns.
1170 Quantification shown on the right. ****P < 0.0001 and **P = 0.0063, Analysis of Variance
1171 (ANOVA). **F.** WT RPE1 cells were transfected with the indicated siRNAs, then treated
1172 with 1.5m M HU for 18 h and assayed for the indicated proteins by WB.
1173
1174 **Figure S3.**
1175 **A.** WT RPE1 cells were transfected with the indicated siRNAs, then treated with 2 mM
1176 HU for 18 h before assaying for the indicated proteins by WB. **B.** Western blots from WT
1177 and SCAI-null U2OS cell lines transfected with the indicated siRNAs and then treated
1178 with 1.5 μM cisplatin for 18 h.
1179
1180 **Figure S4.**
1181 **A.** Western blots from WT and SCAI-null U2OS cell lines transfected with the indicated
1182 siRNAs and then treated with 1.5μM cisplatin for 18 h. **B.** WT RPE1 cells were
1183 transfected with the indicated siRNAs, then treated with 1 mM HU for 18 h and assayed
1184 for the indicated proteins by WB. **C.** P53-null RPE1 parent (Parent), BRCA1-null
1185 (ΔBRCA1), and GFP-WT-BRCA1 Rescue (GFP-BRCA1 Rescue) RPE1 cell lines were
1186 transfected and treated with 1 mM HU for 18 h. WCLs were prepared, and WB were
1187 performed against the indicated proteins. **D.** Western blots from WT, BRCA1/p53-null
1188 (ΔBRCA1), and BRCA1/53BP1-null (ΔBRCA1/Δ53BP1) RPE1 cells transfected with the
1189 indicated siRNAs and then treated with 1.5 mM HU for 18 h. **E.** WT RPE1 and BRCA1-
1190 null cells were transfected with the indicated siRNAs, then treated with 1 mM HU for 18
1191 h and assayed for the indicated proteins by WB. **F.** Western blots against the indicated
1192 proteins from WT and SCAI-null U2OS cells transfected with the specified siRNAs, then
1193 treated with 1.5 μM cisplatin for 18 h.
1194
1195 **Figure S5**

1196 **A.** WT RPE1 cells were transfected with the indicated siRNAs, then treated with 1 mM
1197 HU for 18 h and assayed for the indicated proteins by WB. **B.** Representative images
1198 showing no change in cell cycle distribution in WT RPE1 cells 18 h following treatment
1199 with 27 μM B02 compared to vehicle controls. Quantified on the right, mean ± SD
1200 shown. **C**. Western blots from WT RPE cells transfected with the indicated siRNAs,
1201 pretreated with DMSO, 10 μM Olaparib (Olap), or 27 μM B02, and then treated with 1
1202 mM HU for 18 h.
1203
1204 **Figure S6**
1205 **A** Parent and BRCA1-null RPE1 cells were transfected and then treated with 3 mM HU
1206 for 18 h. Samples were processed for chromatin fraction prior to blotting for the
1207 indicated proteins.
1208

Figure 1

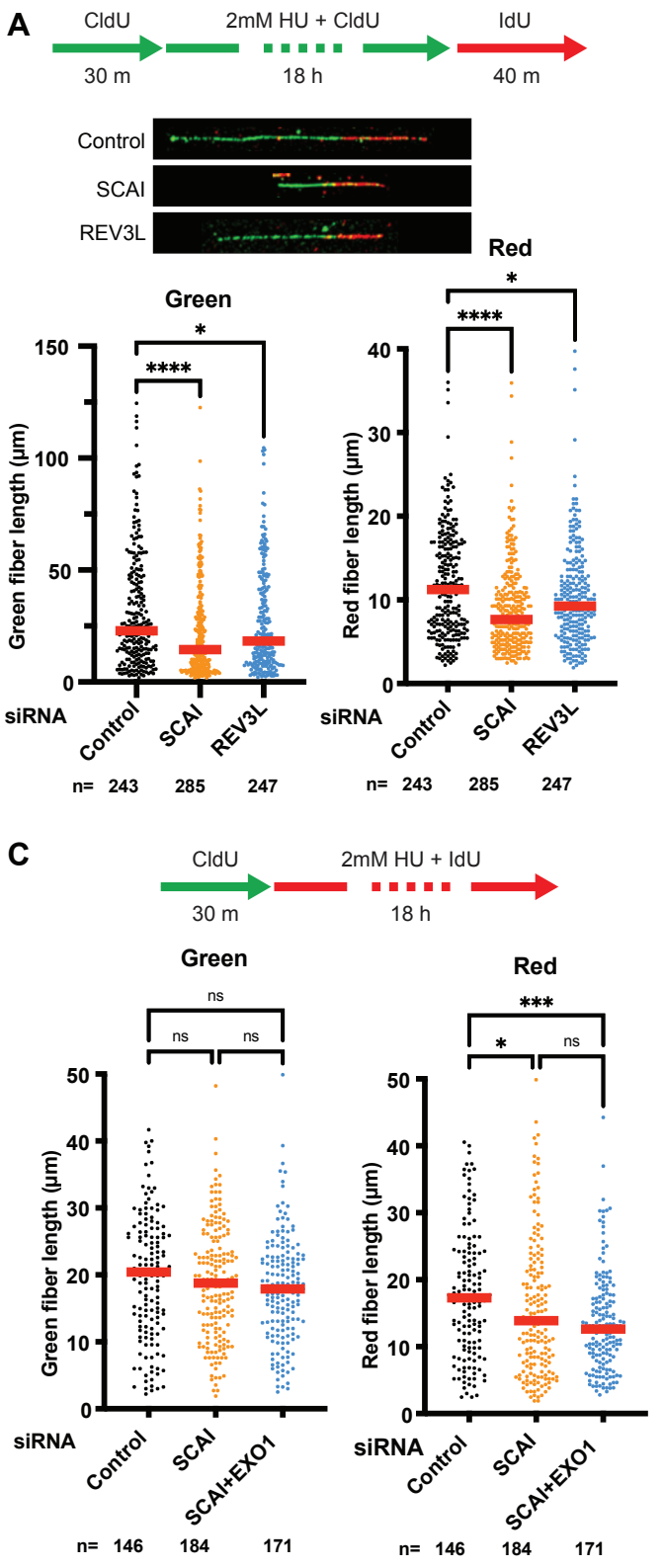
A
CldU
30 m
2mM HU + CldU
18 h
IdU
40 m
Control
SCAI
REV3L
Green
Red
Green fiber length (µm)
Red fiber length (µm)
siRNA
Control
SCAI
REV3L
n= 243 285 247
C
CldU
30 m
2mM HU + IdU
18 h
ns
***
SCAI+EXO1
n= 146 184 171

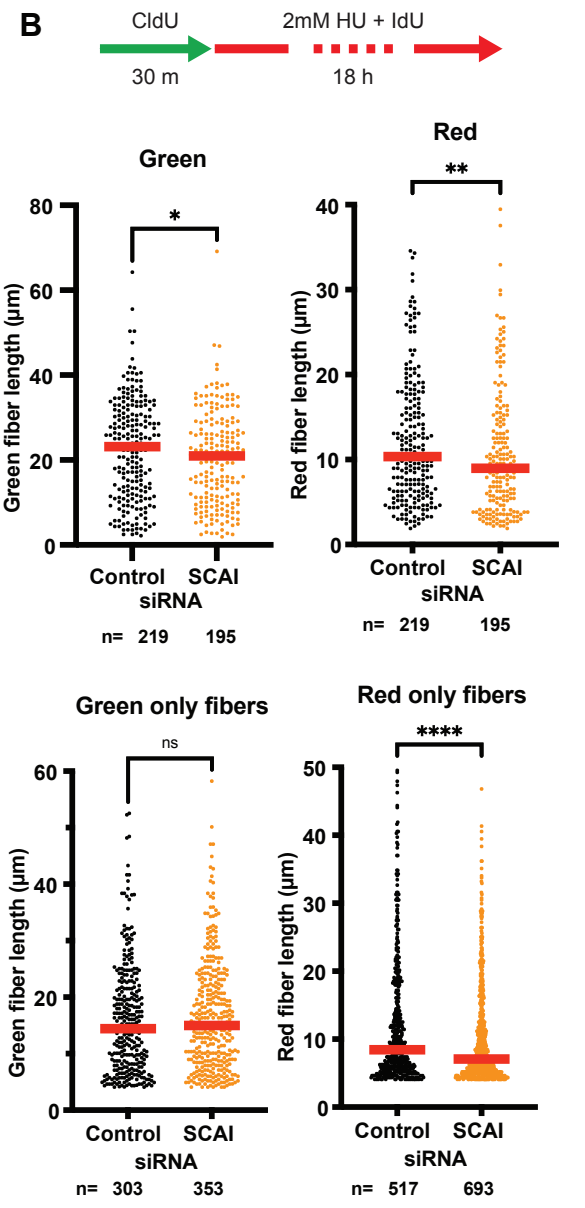
B
CldU
30 m
2mM HU + IdU
18 h
Green
Red
Green fiber length (µm)
Red fiber length (µm)
Control
SCAI
siRNA
n= 219 195
Green only fibers
Red only fibers
ns
****
n= 303 353
n= 517 693

Figure 2

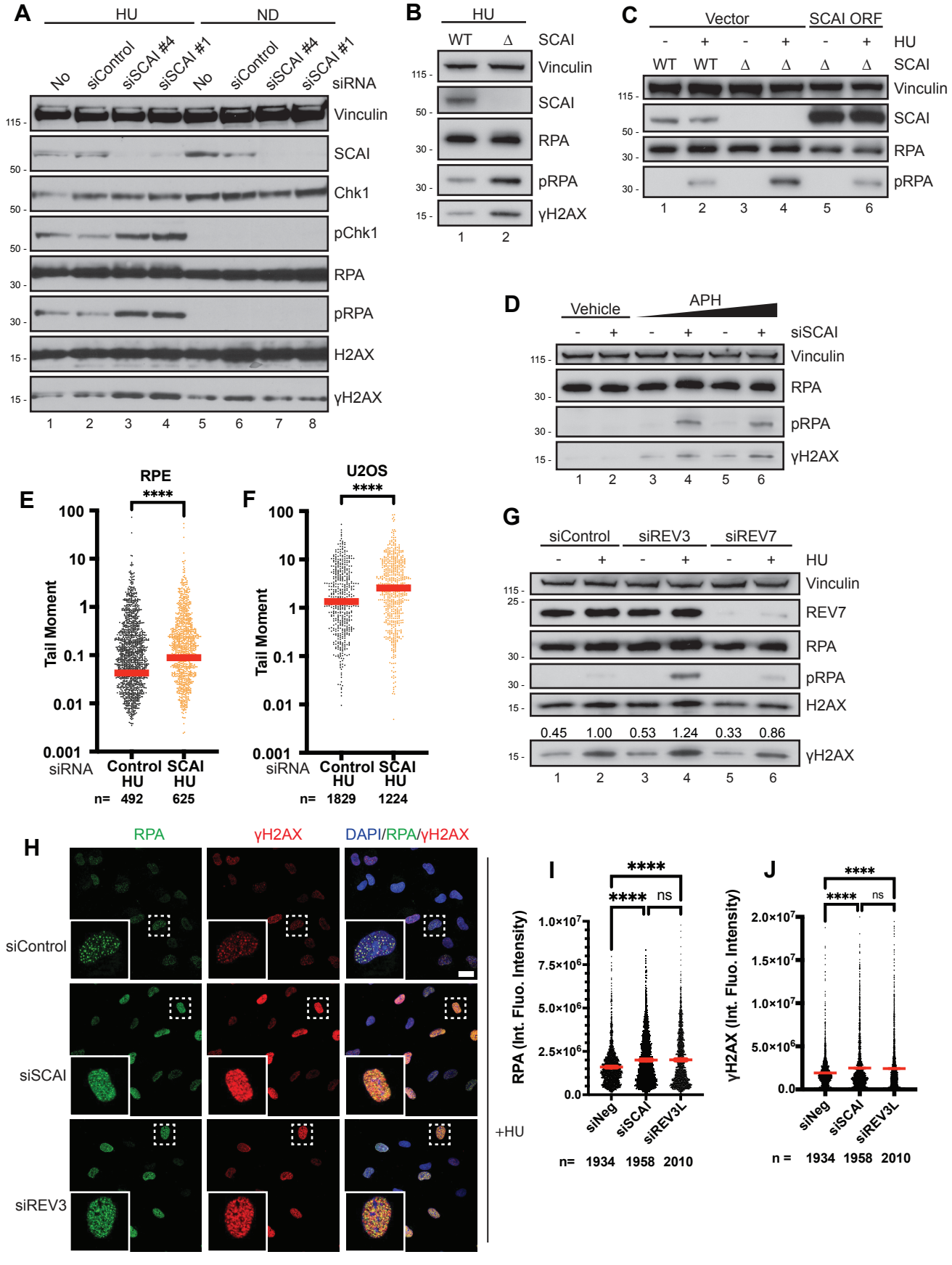
A
HU
ND
No
siControl
siSCAI #4
siSCAI #1
siRNA
Vinculin
SCAI
Chk1
pChk1
RPA
pRPA
H2AX
γH2AX
B
HU
WT
Δ
SCAI
Vinculin
SCAI
RPA
pRPA
γH2AX
C
Vector
SCAI ORF
HU
WT
Δ
SCAI
Vinculin
SCAI
RPA
pRPA
D
Vehicle
APH
siSCAI
Vinculin
RPA
pRPA
γH2AX
E
RPE
****
Tail Moment
siRNA
Control HU
SCAI HU
n= 492 625
F
U2OS
****
Tail Moment
siRNA
Control HU
SCAI HU
n= 1829 1224
G
siControl
siREV3
siREV7
HU
Vinculin
REV7
RPA
pRPA
H2AX
γH2AX
0.45 1.00 0.53 1.24 0.33 0.86
H
RPA
γH2AX
DAPI/RPA/γH2AX
siControl
siSCAI
siREV3
+HU
I
****
****
ns
RPA (Int. Fluo. Intensity)
siNeg
siSCAI
siREV3L
n= 1934 1958 2010
J
****
****
ns
γH2AX (Int. Fluo. Intensity)
siNeg
siSCAI
siREV3L
n = 1934 1958 2010

Figure 3

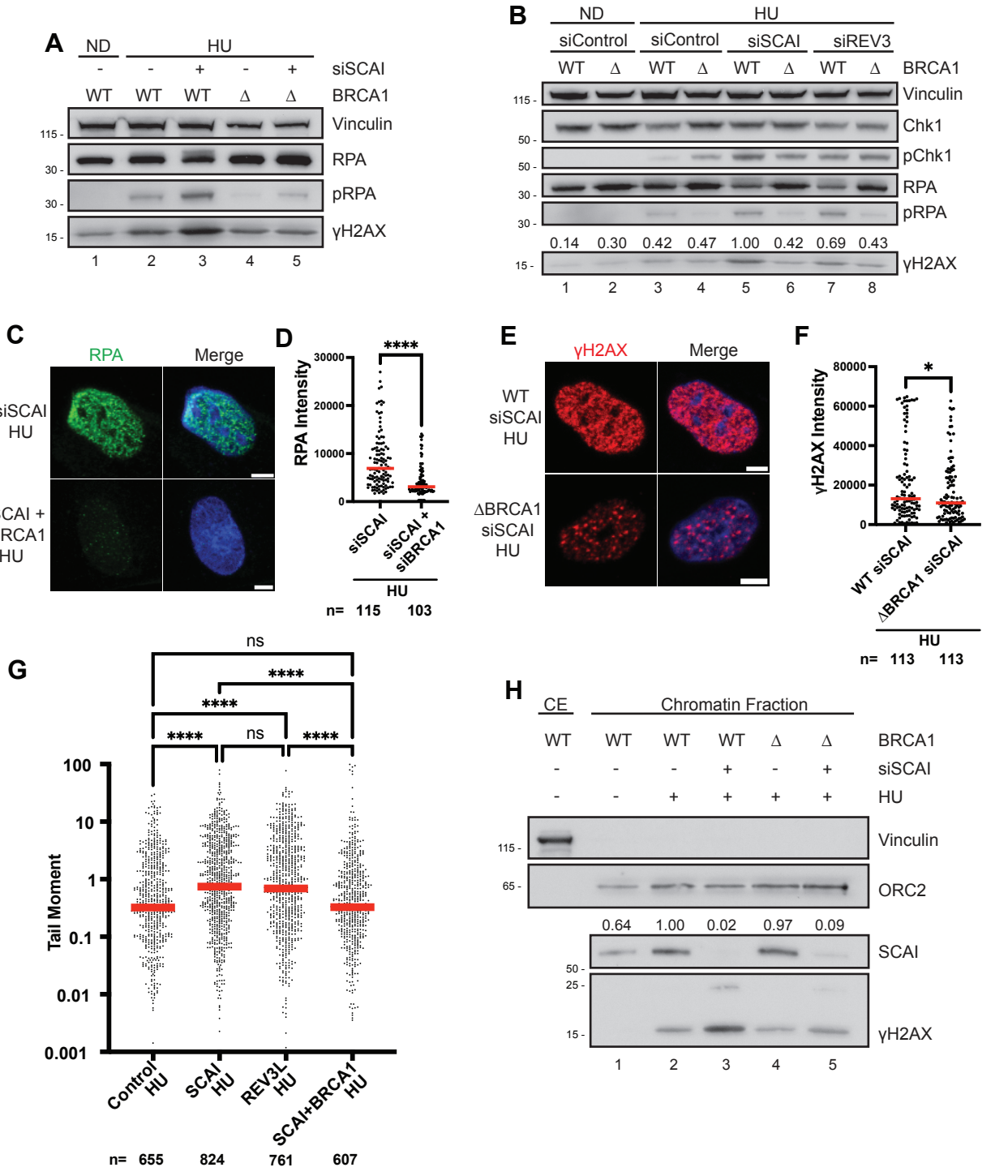
A
ND
HU
siSCAI
BRCA1
WT WT WT Δ Δ
Vinculin
RPA
pRPA
γH2AX
115 -
30 -
30 -
15 -
1 2 3 4 5
B
ND
HU
siControl
siControl
siSCAI
siREV3
BRCA1
Vinculin
Chk1
pChk1
RPA
pRPA
γH2AX
115 -
50 -
50 -
30 -
30 -
15 -
0.14 0.30 0.42 0.47 1.00 0.42 0.69 0.43
1 2 3 4 5 6 7 8
C
RPA
Merge
siSCAI HU
siSCAI + siBRCA1 HU
D
RPA Intensity
30000
20000
10000
0
****
siSCAI
siSCAI + siBRCA1
HU
n= 115 103
E
γH2AX
Merge
WT siSCAI HU
ΔBRCA1 siSCAI HU
F
γH2AX Intensity
80000
60000
40000
20000
0
*
WT siSCAI
ΔBRCA1 siSCAI
HU
n= 113 113
G
ns
****
****
****
ns
****
Tail Moment
100
10
1
0.1
0.01
0.001
Control HU
SCAI HU
REV3L HU
SCAI+BRCA1 HU
n= 655 824 761 607
H
CE
Chromatin Fraction
WT WT WT WT Δ Δ
BRCA1
siSCAI
HU
Vinculin
ORC2
SCAI
γH2AX
115 -
65 -
50 -
25 -
15 -
0.64 1.00 0.02 0.97 0.09
1 2 3 4 5

Figure 4

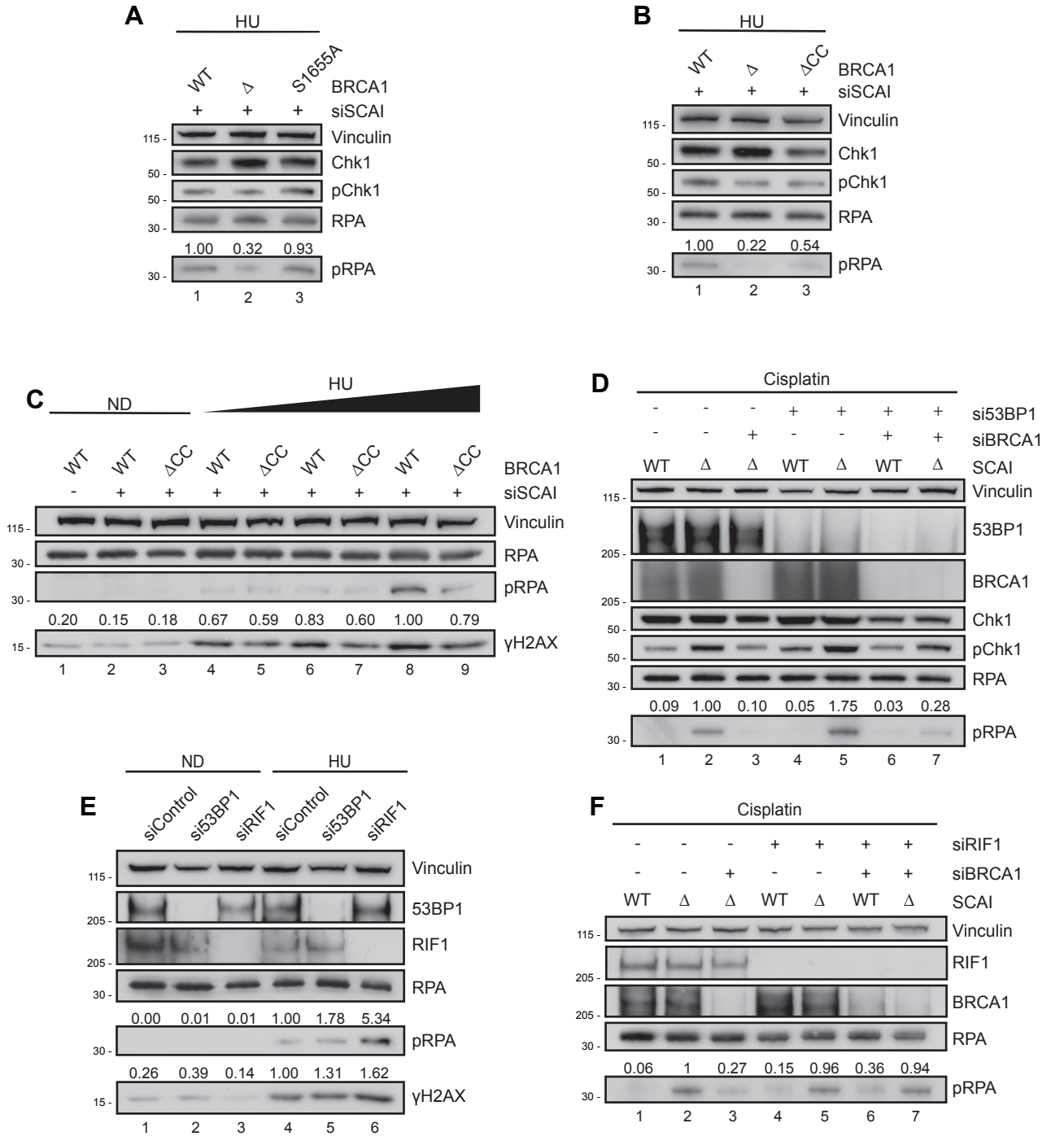
A
HU
WT
Δ
S1655A
BRCA1
siSCAI
Vinculin
Chk1
pChk1
RPA
1.00 0.32 0.93
pRPA
1 2 3
B
HU
WT
Δ
ΔCC
BRCA1
siSCAI
Vinculin
Chk1
pChk1
RPA
1.00 0.22 0.54
pRPA
1 2 3
C
ND
HU
WT WT ΔCC WT ΔCC WT ΔCC WT ΔCC
BRCA1
siSCAI
Vinculin
RPA
pRPA
0.20 0.15 0.18 0.67 0.59 0.83 0.60 1.00 0.79
γH2AX
1 2 3 4 5 6 7 8 9
D
Cisplatin
si53BP1
siBRCA1
WT Δ Δ WT Δ WT Δ
SCAI
Vinculin
53BP1
BRCA1
Chk1
pChk1
RPA
0.09 1.00 0.10 0.05 1.75 0.03 0.28
pRPA
1 2 3 4 5 6 7
E
ND
HU
siControl si53BP1 siRIF1 siControl si53BP1 siRIF1
Vinculin
53BP1
RIF1
RPA
0.00 0.01 0.01 1.00 1.78 5.34
pRPA
0.26 0.39 0.14 1.00 1.31 1.62
γH2AX
1 2 3 4 5 6
F
Cisplatin
siRIF1
siBRCA1
WT Δ Δ WT Δ WT Δ
SCAI
Vinculin
RIF1
BRCA1
RPA
0.06 1 0.27 0.15 0.96 0.36 0.94
pRPA
1 2 3 4 5 6 7

Figure 5

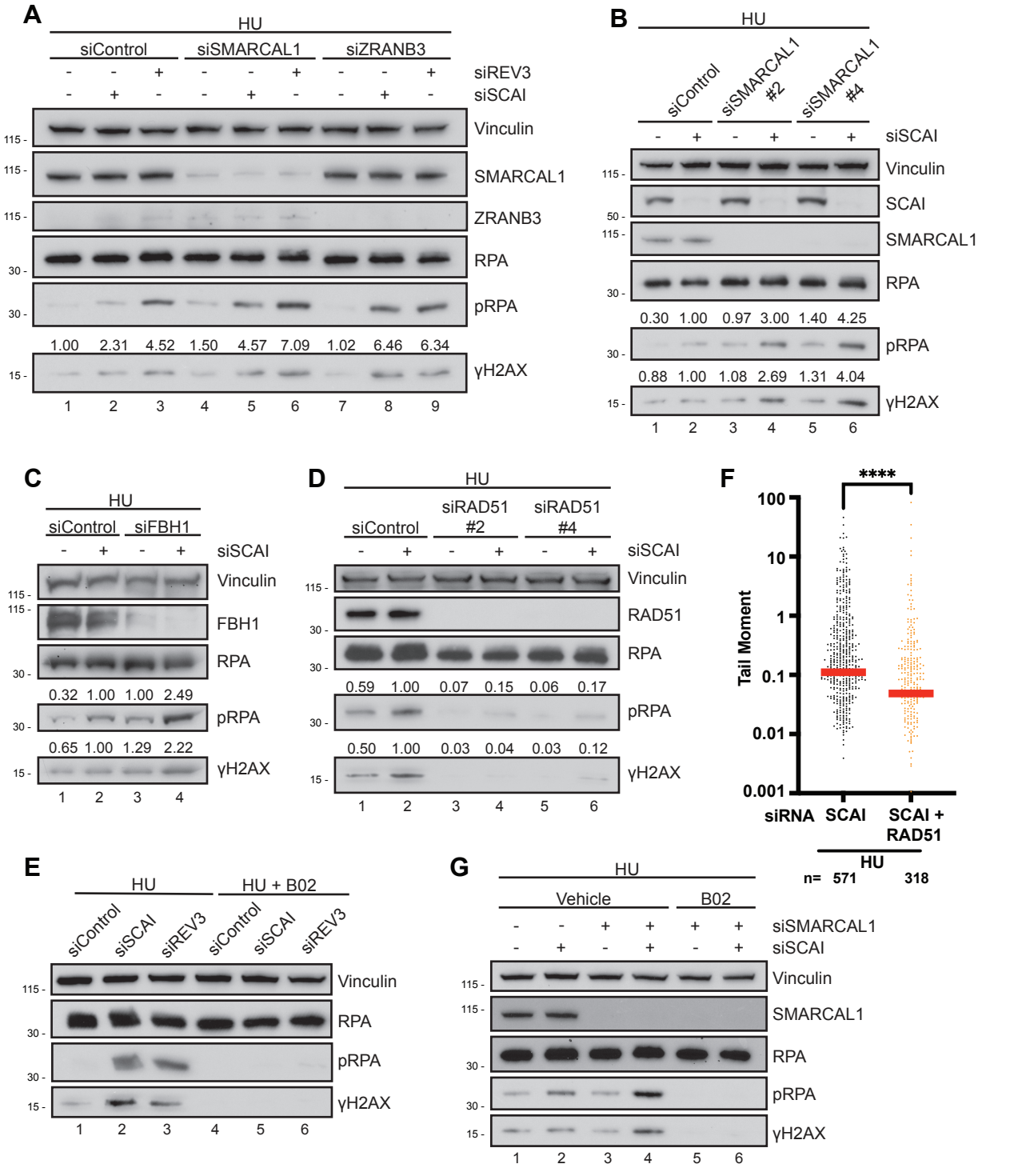
A
HU
siControl
siSMARCAL1
siZRANB3
siREV3
siSCAI
Vinculin
SMARCAL1
ZRANB3
RPA
pRPA
1.00 2.31 4.52 1.50 4.57 7.09 1.02 6.46 6.34
γH2AX
1 2 3 4 5 6 7 8 9
B
HU
siControl
siSMARCAL1 #2
siSMARCAL1 #4
siSCAI
Vinculin
SCAI
SMARCAL1
RPA
0.30 1.00 0.97 3.00 1.40 4.25
pRPA
0.88 1.00 1.08 2.69 1.31 4.04
γH2AX
1 2 3 4 5 6
C
HU
siControl
siFBH1
siSCAI
Vinculin
FBH1
RPA
0.32 1.00 1.00 2.49
pRPA
0.65 1.00 1.29 2.22
γH2AX
1 2 3 4
D
HU
siControl
siRAD51 #2
siRAD51 #4
siSCAI
Vinculin
RAD51
RPA
0.59 1.00 0.07 0.15 0.06 0.17
pRPA
0.50 1.00 0.03 0.04 0.03 0.12
γH2AX
1 2 3 4 5 6
F
****
Tail Moment
100
10
1
0.1
0.01
0.001
siRNA
SCAI
SCAI + RAD51
HU
n= 571 318
E
HU
HU + B02
siControl
siSCAI
siREV3
siControl
siSCAI
siREV3
Vinculin
RPA
pRPA
γH2AX
1 2 3 4 5 6
G
HU
Vehicle
B02
siSMARCAL1
siSCAI
Vinculin
SMARCAL1
RPA
pRPA
γH2AX
1 2 3 4 5 6

Figure 6

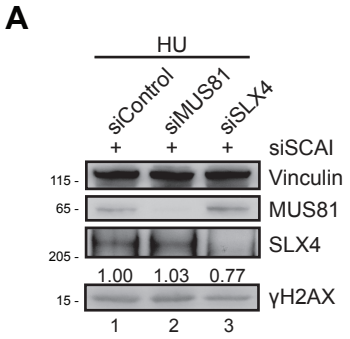
A
HU
siControl
siMUS81
siSLX4
siSCAI
+ + +
115 -
Vinculin
65 -
MUS81
205 -
SLX4
1.00 1.03 0.77
15 -
γH2AX
1 2 3

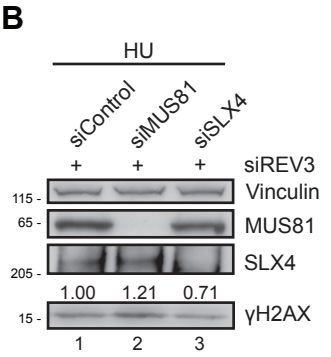
B
HU
siControl
siMUS81
siSLX4
siREV3
+ + +
115 -
Vinculin
65 -
MUS81
205 -
SLX4
1.00 1.21 0.71
15 -
γH2AX
1 2 3

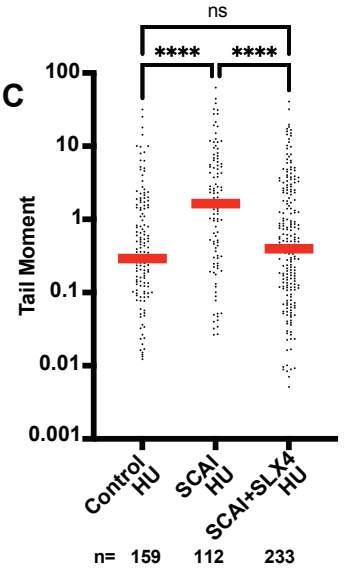
C
ns
****
****
Tail Moment
100
10
1
0.1
0.01
0.001
Control HU
SCAI HU
SCAI+SLX4 HU
n= 159 112 233

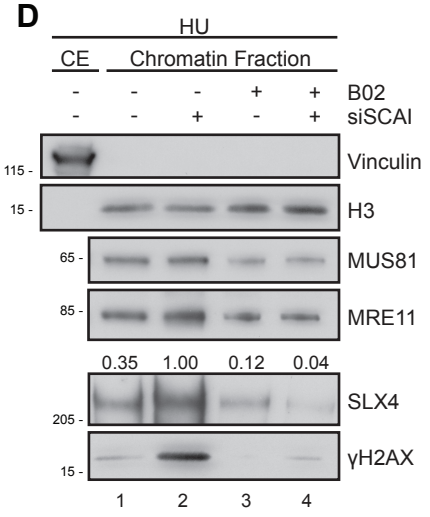
D
HU
CE
Chromatin Fraction
B02
siSCAI
115 -
Vinculin
15 -
H3
65 -
MUS81
85 -
MRE11
0.35 1.00 0.12 0.04
205 -
SLX4
15 -
γH2AX
1 2 3 4

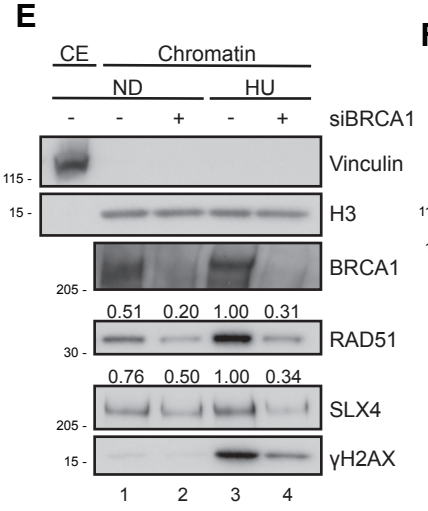
E
CE
Chromatin
ND
HU
siBRCA1
115 -
Vinculin
15 -
H3
205 -
BRCA1
0.51 0.20 1.00 0.31
30 -
RAD51
0.76 0.50 1.00 0.34
205 -
SLX4
15 -
γH2AX
1 2 3 4

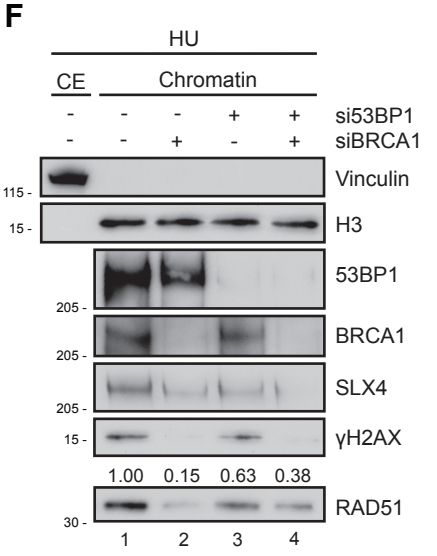
F
HU
CE
Chromatin
si53BP1
siBRCA1
115 -
Vinculin
15 -
H3
205 -
53BP1
205 -
BRCA1
205 -
SLX4
15 -
γH2AX
1.00 0.15 0.63 0.38
30 -
RAD51
1 2 3 4

Figure 7

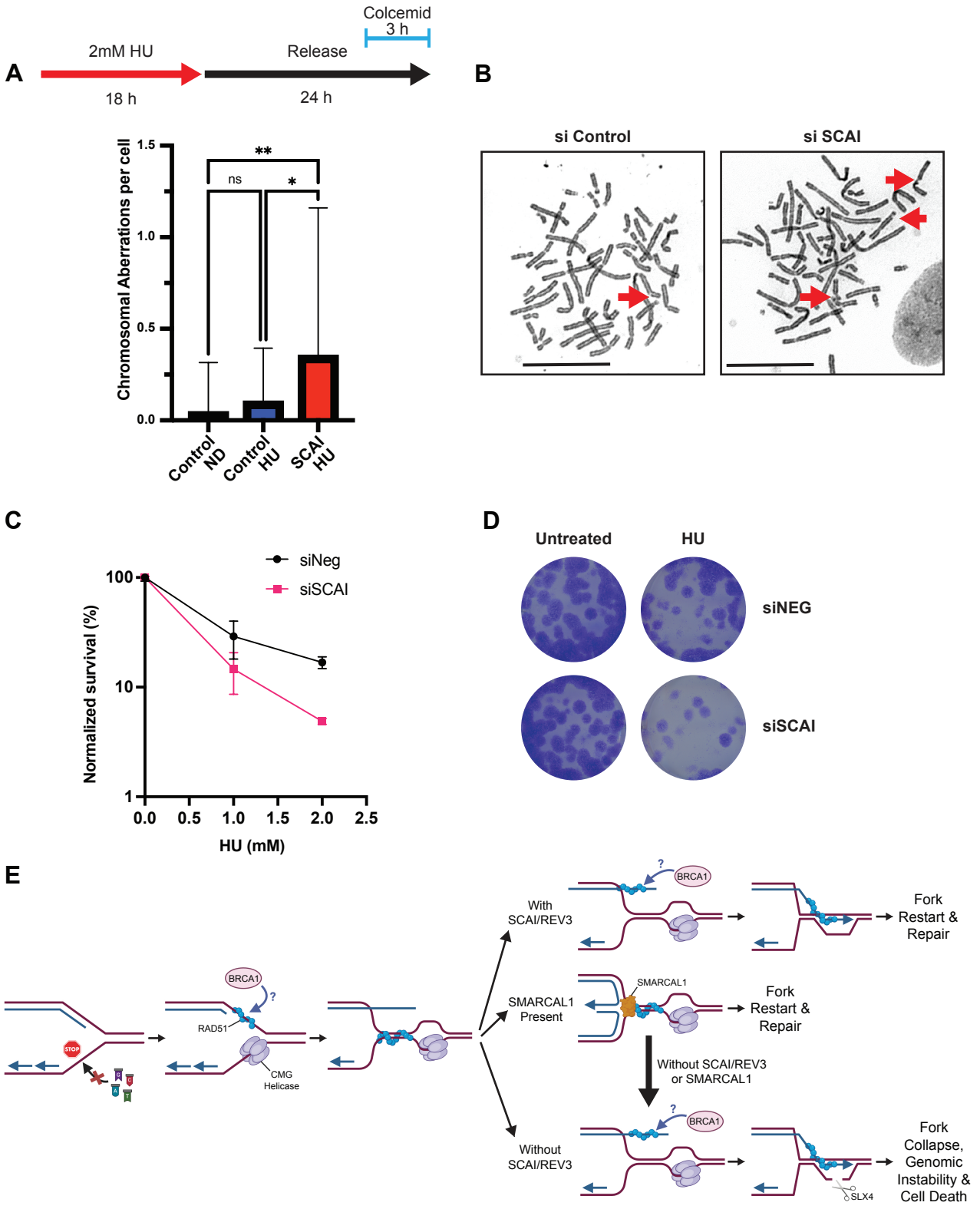
A
2mM HU
18 h
Release
24 h
Colcemid
3 h
Chromosomal Aberrations per cell
1.5
1.0
0.5
0.0
**
ns
*
Control ND
Control HU
SCAI HU
B
si Control
si SCAI
C
siNeg
siSCAI
Normalized survival (%)
100
10
1
0.0
0.5
1.0
1.5
2.0
2.5
HU (mM)
D
Untreated
HU
siNEG
siSCAI
E
STOP
BRCA1
RAD51
CMG Helicase
With SCAI/REV3
SMARCAL1 Present
SMARCAL1
Fork Restart & Repair
Without SCAI/REV3 or SMARCAL1
Without SCAI/REV3
SLX4
Fork Collapse, Genomic Instability & Cell Death